CHALMERS
FINITE ELEMENT CENTER

PREPRINT 2003-10

Generalized Green's Functions and the Effective Domain of Influence

Donald Estep, Michael Holst, and Mats G. Larson

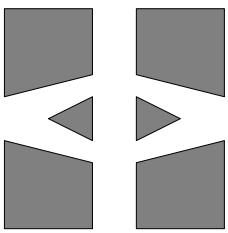

Chalmers Finite Element Center
CHALMERS UNIVERSITY OF TECHNOLOGY
Göteborg Sweden 2003

CHALMERS FINITE ELEMENT CENTER

Preprint 2003-10

Generalized Green's Functions and the Effective Domain of Influence

Donald Estep, Michael Holst, and Mats G. Larson

CHALMERS

Chalmers Finite Element Center
Chalmers University of Technology
SE–412 96 Göteborg Sweden
Göteborg, October 2003

Generalized Green's Functions and the Effective Domain of Influence
Donald Estep, Michael Holst, and Mats G. Larson
NO 2003-10
ISSN 1404–4382

Chalmers Finite Element Center
Chalmers University of Technology
SE–412 96 Göteborg
Sweden
Telephone: +46 (0)31 772 1000
Fax: +46 (0)31 772 3595
www.phi.chalmers.se

Printed in Sweden
Chalmers University of Technology
Göteborg, Sweden 2003

GENERALIZED GREEN'S FUNCTIONS AND THE EFFECTIVE DOMAIN OF INFLUENCE

DONALD ESTEP *, MICHAEL HOLST †, AND MATS LARSON ‡

Abstract. One well-known approach to *a posteriori* analysis of finite element solutions of elliptic problems estimates the error in a quantity of interest in terms of residuals and a generalized Green's function. The generalized Green's function, which solves the adjoint problem with data related to the quantity of interest, measures the effects of stability on the accuracy of the approximation. In particular, the decay of influence characteristic to elliptic problems is reflected in the behavior of the Green's functions. In this paper, we show that consideration of the behavior of the generalized Green's function can be used to improve the efficiency of the solution process. This possibility arises when the goal is to compute multiple quantities of interest and/or to compute quantities of interest that involve globally-supported information of the solution, as with average values and norms. In the latter case, we introduce a decomposition of solution to localize the global computation in which we solve a set of problems involving localized information, and then recover the desired information by combining the local solutions. By treating each computation of a quantity of interest as an independent computation, we can lower the maximum number of elements required to achieve the desired accuracy to a significant extent.

Key words. *a posteriori* error estimates, adaptive error control, adaptive mesh refinement, adjoint problem, coarse-grained parallelization, decay of influence, domain decomposition, effective domain of influence, dual problem, efficient discretization, elliptic problem, error estimates, finite element method, generalized Green's function, localization, residual error, solution decomposition, stability, variational analysis

AMS subject classifications. 65N15, 65N30, 65N50

1. Introduction.

A characteristic property of elliptic partial differential equations is a *global* domain of influence. That is, a local perturbation of data near one point affects the solution of an elliptic equation throughout the domain of the problem. Indeed, in the extreme case of an analytic harmonic function, prescribing the values of a solution on any small sub-domain or even on a piece of curve suffices to define its values throughout the domain. Of course, this property has profound consequences for the numerical solution of elliptic equations.

Yet when taken out of context, this property can give a misleading picture. In particular, elliptic problems often have the property that the strength of the effect of a localized perturbation on a solution decays significantly with the distance from the support of the perturbation, at least in some directions. It turns out that this property also has profound consequences for the numerical solution of elliptic problems. We explore some of the consequences in this paper.

A simple way to see the decay of influence in an elliptic problem is to consider the properties of fundamental solutions and the related Green's functions. If $L(D)$ is a constant coefficient differential operator on $\mathbb{R}^d$, $d \geq 1$, then a fundamental solution for L is a distribution $K(x)$ satisfying

$$L(D)K(x) = \delta_0(x), \quad x \in \mathbb{R}^d, \tag{1.1}$$

where δ_y denotes the delta distribution at a point y, i.e., $(\delta_y, \phi) = \phi(y)$ for all smooth, integrable functions ϕ, with $(\ ,\ )$ denoting the L^2 inner product on the domain in question. We interpret (1.1) in a weak sense, and the Malgrange-Ehrenpreis Theorem ([14]) guarantees that K exists. With this definition, we have

$$L(D)(K * f) = (L(D)K) * f = \delta_0 * f = f(x),$$

*Department of Mathematics, Colorado State University, Fort Collins, CO 80523, USA. (estep@math.colostate.edu). The research of D. Estep is partially supported by the National Science Foundation, DMS-9805748 and DMS-0107832.

†Michael Holst, Department of Mathematics, University of California, San Diego, 9500 Gilman Drive, Dept. 0112, La Jolla, CA 92093-0112 USA. (mholst@math.ucsd.edu). The research of M. Holst is partially supported in by the National Science Foundation, CAREER Award 9875856, and by a UCSD Hellman Fellowship.

‡Department of Mathematics, Chalmers University of Technology, S41296 Göteborg, Sweden. (mgl@math.chalmers.se). The research of M. Larson is partially supported by the Swedish Research Council.

as long as the convolution

$$K * f = \int_{\mathbb{R}^d} K(x-y)f(y)\,dy$$

is defined. In other words, the solution of

$$L(D)u(x) = f(x), \quad x \in \mathbb{R}^d,$$

is given by

$$u = K * f. \tag{1.2}$$

Now in the case of the Laplacian, $L(D) = -\Delta$, in $\mathbb{R}^3$, the fundamental solution is

$$K(x) = \frac{1}{4\pi|x|},$$

where $|x|$ denotes the Euclidean norm of x. Suppose that u solves

$$-\Delta u(x) = f(x), \quad x \in \mathbb{R}^3,$$

and the data f is perturbed by a continuous function δf with compact support $\text{supp}(\delta f)$. We consider the resulting perturbation δu to the value of u at a point x located some distance from $\text{supp}(\delta f)$, i.e. $\text{dist}\,(x, \text{supp}(\delta f)) > 0$. It follows that

$$|\delta u(x)| = \frac{1}{4\pi}\left|\int_{\mathbb{R}^3} \frac{\delta f(y)}{|x-y|}\,dy\right| \leq \frac{\max|\delta f| \,\times\, \text{volume of supp}(\delta f)}{4\pi\,\text{dist}\,(x, \text{supp}(\delta f))}.$$

As x moves away from $\text{supp}(\delta f)$, the solution is affected by the perturbation less and less.

Green's functions play the role of fundamental solutions for boundary value problems on finite domains. Central to the definition of a Green's function is the notion of the adjoint operator. If $L(D,x)$ is a linear differential operator, then the adjoint operator $L^*(D,x)$ satisfies

$$(L(D,\cdot)u(\cdot), v(\cdot)) = (u(\cdot), L^*(D,\cdot)v(\cdot)) \tag{1.3}$$

for all smooth functions u, v with compact support. For example, if

$$L(D,x)u = -\nabla\cdot a(x)\nabla u + b(x)\cdot\nabla u + c(x)u(x),$$

where $u : \mathbb{R}^d \to \mathbb{R}$, a is a $d \times d$ matrix function of x, b is a d-vector function of x, and c is a function of x, then

$$L^*(D,x)v = -\nabla\cdot a(x)\nabla v - \text{div}\,(b(x)v) + c(x)v(x).$$

More generally using the multi-index notation, if $L(D,x)u = \sum_{|\alpha|\leq m} a_\alpha D^\alpha u$, then $L^*(D,x)v = \sum_{|\alpha|\leq m}(-1)^{|\alpha|}D^\alpha\big(a_\alpha v\big)$.

Now on a finite domain Ω with no assumption of compact support, the integration by parts (1.3) that defines the adjoint yields generally nonzero boundary integrals over the boundary $\partial\Omega$. The Green's function is a solution of the adjoint differential equation chosen to yield the analog of the representation (1.2) and to simplify these boundary integrals. To fix ideas, we assume that $L(D,x)$ is a second order elliptic operator and consider the Dirichlet problem,

$$\begin{cases} L(D,x)u(x) = f(x), & x \in \Omega, \\ u(x) = 0, & x \in \partial\Omega, \end{cases} \tag{1.4}$$

where Ω is a convex smooth or polygonal domain in $\mathbb{R}^d$, $d = 2$ or 3, and the coefficients of L and the data f are suitably smooth. Suppose that $y \in \Omega$. The Green's function $G(y, x)$ satisfies the adjoint boundary value problem,

$$\begin{cases} L^*(D, x)G(y, x) = \delta_y(x), & x \in \Omega, \\ G(y, x) = 0, & x \in \partial\Omega. \end{cases} \tag{1.5}$$

Because of the boundary conditions in (1.4) and (1.5), we have

$$\big(f(\cdot), G(y, \cdot)\big) = \big(L(D, \cdot)u(\cdot), G(y, \cdot)\big) = \big(u(\cdot), L^*(D, \cdot)G(y, \cdot)\big) = \big(u, \delta_y\big) = u(y), \tag{1.6}$$

for $y \in \Omega$. In other words, the solution of (1.4) is given by

$$u(x) = \int_\Omega G(x, z)f(z)\, dz, \quad x \in \Omega. \tag{1.7}$$

In this paper, we are concerned with the effects of perturbations on the data (in the form of discretization). If we perturb the data f to get new data $\tilde{f}$, and let $\tilde{u}$ denote the solution of (1.4) with data $\tilde{f}$ replacing f, we obtain

$$u(x) - \tilde{u}(x) = \int_\Omega G(x, z)(f(z) - \tilde{f}(z))\, dz, \quad x \in \Omega. \tag{1.8}$$

REMARK 1.1. *In order to derive the analog of the representation (1.7) for a general elliptic operator posed together with general boundary conditions, we must choose suitable adjoint boundary conditions to go with the adjoint operator. These boundary conditions are chosen, if possible, so that the boundary integrals arising from the integration in parts in (1.6) that involve unknown values of the solution vanish. The remaining boundary integrals appear on the right-hand side of the resulting analog of (1.7). The simplest example is*

$$\begin{cases} -\Delta u(x) = f(x), & x \in \Omega, \\ u(x) = g(x), & x \in \partial\Omega, \end{cases}$$

for which the Green's function solves,

$$\begin{cases} -\Delta G(y, x) = \delta_y(x), & x \in \Omega, \\ G(y, x) = 0, & x \in \partial\Omega, \end{cases}$$

for $y \in \Omega$, and u is represented by

$$u(y) = \int_\Omega G(y, x)f(x)\, dx + \int_{\partial\Omega} g(x)\partial_{n_x} G(y, x)\, dS_x,$$

where ∂_{n_x} denotes the normal derivative on the boundary $\partial\Omega$ (with respect to x) and the second integral on the right is a surface integral. See [20] for a discussion of more general cases.

Standard elliptic theory yields the existence of the solution G of (1.5). In fact, in the case of a constant coefficient differential operator $L(D)$,

$$G(y, x) = K(y - x) + \mathcal{G}(y, x), \quad x, y \in \Omega,$$

where for each $x \in \Omega$, $\mathcal{G}(y, x)$ is the solution of the Dirichlet problem,

$$\begin{cases} L(D_y)\mathcal{G}(y, x) = 0, & y \in \Omega, \\ \mathcal{G}(y, x) = -K(y - x), & y \in \partial\Omega, \end{cases}$$

with D_y denoting differentiation with respect to y. Thus in the case of a constant coefficient differential operator, the Green's function is a fundamental solution chosen to have "suitable"

values on the boundary of the finite domain Ω. In particular, the singular behavior of the Green's function is determined by the singular behavior of the fundamental solution.

In general, determining an explicit formula for a particular Green's function is difficult, if not impossible. However, we can determine the Green's function in a few cases. For example, the Green's function for the Dirichlet problem for the Laplacian,

$$\begin{cases} -\Delta u(x) = f(x), & x \in \Omega, \\ u(x) = 0, & x \in \partial\Omega, \end{cases}$$

where Ω is a ball of radius r centered at the origin, is

$$G(y,x) = \frac{1}{4\pi} \times \begin{cases} |y-x|^{-1} - r|y|^{-1}\left|\frac{r^2 y}{|y|^2} - x\right|^{-1}, & y \neq 0, \\ |x|^{-1} - r^{-1}, & y = 0, \end{cases}$$

in $\mathbb{R}^3$, and

$$G(y,x) = \frac{1}{2\pi} \times \begin{cases} \ln\left(\frac{|y|\left|\frac{r^2 y}{|y|^2} - x\right|}{r|y-x|}\right), & y \neq 0, \\ \ln\left(\frac{r}{|x|}\right), & y = 0, \end{cases} \tag{1.9}$$

in $\mathbb{R}^2$. If the data f is perturbed by a continuous function δf with compact support $\operatorname{supp}(\delta f) \subset \Omega$, then a simple geometrical argument shows that

$$|y-x| \leq \left|\frac{r^2 y}{|y|^2} - x\right|, \quad x \in \operatorname{supp}(\delta f),\ y \in \Omega \setminus \operatorname{supp}(\delta f).$$

In the case of $\mathbb{R}^3$, arguing as above, we conclude that the perturbation in the value of the solution corresponding to δf is bounded as

$$|\delta u(y)| \leq \frac{\max|\delta f| \times \text{ volume of } \operatorname{supp}(\delta f) \times \left(1 + \frac{r}{|y|}\right)}{4\pi \operatorname{dist}(y, \operatorname{supp}(\delta f))}.$$

Again, we see that the effects of a local perturbation in the data decays with the distance from the support of the perturbation.

In this paper, we explore the consequences of the decay of influence inherent to elliptic problems for the numerical solution of such equations. Our chief tool is a variational *a posteriori* error analysis that involves an generalization of the notion of a Green's function. This generalized Green's function determines the propagation and decay of influence of discretization error in a quantity of interest computed from the numerical solution. Using the information obtained from the generalized Green's function, we define the notion of an *effective* domain of influence. In order to achieve accuracy in the desired quantity, a mesh must be sufficiently refined inside the effective domain of influence, while outside the effective domain, the mesh may be relatively coarse. This turns out to have very useful consequences for the efficient and accurate computation of numerical solutions.

We begin in Sec. 2 with a simple example of a finite element discretization of Poisson's equation in a disk. The analysis leading to a decay of influence result for a finite element discretization is different than the general analysis presented above because of the cancellation of errors inherent to a Galerkin discretization. We use this simple example to illustrate the differences. Using the *a posteriori* analysis together with formula for the Green's function for the Laplacian in the disk, we show that the error in the energy norm in a small region is affected relatively little by discretization errors committed away from the region. This means we can compute a numerical solution with accurate values in a small region using a mesh that is fine near the region and coarse away from the region. The effective domain of influence is the region requiring the fine mesh.

In Sec. 3, we present the *a posteriori* error analysis for a finite element approximation of a general linear elliptic problem. This analysis uses the generalized Green's function, which allows

the estimation of the error in a desired quantity computed as a linear functional of the solution. We explain how information about the generalized Green's function can be used in an adaptive error control algorithm to produce an accurate and efficiently refined mesh. Unlike the example in Sec. 2, it is usually impossible to find an explicit formula for the generalized Green's function. Therefore, we discuss the approximation of the generalized Green's function by numerical solution of the adjoint problem. Finally, we define the effective domain of influence.

In Sec. 4, we explain how the problem of computing multiple quantities of interest simultaneously arises naturally in practice and also when the data for the generalized Green's function does not have spatially localized support. In that case, we introduce a partition of unity to localize the data for the generalized Green's function and, in effect, to decompose the solution process. In Sec. 5, we then explain how explicit knowledge of the effective domains of influence corresponding to multiple quantities of interest can be used to compute the solution efficiently.

The solution decomposition introduced in Sec. 4 raises the two issues of identifying the effective domain of influence in terms of a given mesh and recognizing whether two effective domains of influence are more-or-less distinct or not. We address these issues in Sec. 6.

Finally, we present several computational examples illustrating these ideas in Sec. 7 and conclude in Sec. 8.

Acknowledgements. The authors gratefully thank James Stewart, Sandia National Laboratories and Simon Tavener, Colorado State University for their comments on an early draft of this paper.

2. The Green's function and the error of a finite element solution of Poisson's equation in a disk. In this section, we analyze a simple example of a finite element discretization of Poisson's equation in a circle. First, some notation. For a region Ω in $\mathbb{R}^d$, $d = 2, 3$, we use $L^2(\Omega)$ to denote the space of square integrable functions with inner product, $(u, v) = (u, v)_\Omega = \int_\Omega u \cdot v \, dx$, and corresponding norm $\|u\| = \|u\|_\Omega = (u, u)^{1/2}$, with the obvious interpretation for scalar or vector valued functions. We use $H^p(\Omega)$ to denote the space of functions that are in $L^2(\Omega)$ and whose derivatives up to order p are in $L^2(\Omega)$, with the usual norm. We use $H_0^1(\Omega)$ to denote the subspace of $H^1(\Omega)$ consisting of functions that are zero on the boundary $\partial\Omega$ of Ω. We also use the seminorm, $|v|_{1,\Omega} = \|\nabla v\|_\Omega$.

We let Ω denote the disk of radius r centered at the origin in $\mathbb{R}^2$, and consider the Dirichlet problem

$$\begin{cases} -\Delta u(x) = f(x), & x \in \Omega, \\ u(x) = 0, & x \in \partial\Omega, \end{cases} \tag{2.1}$$

where f is, say, continuous. Introducing the bilinear form, $A(v, w) = (\nabla v, \nabla w)$, the equivalent weak formulation of (2.1) is:

$$\text{Find } u \in H_0^1(\Omega) \text{ such that } A(u, v) = (f, v) \text{ for all } v \in H_0^1(\Omega).$$

To construct a finite element discretization, we form a piecewise polygonal approximation of $\partial\Omega$ whose nodes lie on $\partial\Omega$ and which is contained inside Ω. This forms the boundary of a convex polygonal domain Ω_h. We let $\mathcal{T}_h$ denote a simplex triangulation of Ω_h that is locally quasi-uniform. We let h_K denote the length of the longest edge of $K \in \mathcal{T}_h$ and define the piecewise constant mesh function h by $h(x) = h_K$ for $x \in K$. We also use h to denote $\max_K h_K$. We choose a finite element solution from the space V_h of functions that are continuous on Ω, piecewise linear on Ω_h with respect to $\mathcal{T}_h$, zero on the boundary $\partial\Omega_h$, and finally extended to be zero in the region $\Omega \setminus \Omega_h$. With this construction, we have $V_h \subset H_0^1(\Omega)$, and for smooth functions, the error of interpolation into V_h is $\mathbf{O}(h^2)$ in $\| \, \|$, but not better (see [19]). The finite element method is:

$$\text{Compute } U \in V_h \text{ such that } A(U, v) = (f, v) \text{ for all } v \in V_h. \tag{2.2}$$

Suppose that ω is a small region contained in Ω located well away from $\partial\Omega$ and that we wish to estimate the error $e = u - U$ in the energy norm in ω, i.e., $\|e\|_{1,\omega}$. We use the *a posteriori* error

analysis introduced in [8] closely. With $H^{-1}(\omega)$ denoting the dual space to $H^1(\omega)$ and $\| \|_{-1,\omega}$ the associated norm, we can evaluate the norm variationally as

$$\|e\|_{1,\omega} = \sup_{\substack{\psi \in H^{-1}(\omega) \\ \|\psi\|_{-1,\omega}=1}} (e, \psi). \tag{2.3}$$

The supremum is achieved for some $\psi \in H^{-1}(\omega)$. We extend this ψ to $H^{-1}(\Omega)$ by setting it to zero in $\Omega \setminus \omega$. Let ϕ solve the adjoint, or dual, problem:

$$\text{Find } \phi \in H_0^1(\Omega) \text{ such that } A(v, \phi) = (v, \psi) \text{ for all } v \in H_0^1(\Omega).$$

We obtain

$$\begin{aligned}
\|e\|_{1,\omega} &= (e, \psi) = A(e, \phi) \\
&= \int_\Omega \nabla e \cdot \nabla \phi \, dx = \int_\Omega \nabla u \cdot \nabla \phi \, dx - \int_\Omega \nabla U \cdot \nabla \phi \, dx \\
&= \int_\Omega f \phi \, dx - \int_\Omega \nabla U \cdot \nabla \phi \, dx.
\end{aligned}$$

Using the Galerkin orthogonality (2.2), we obtain the **error representation formula**,

$$\|e\|_{1,\omega} = \int_\Omega f(\phi - \pi_h \phi) \, dx - \int_\Omega \nabla U \cdot \nabla(\phi - \pi_h \phi) \, dx, \tag{2.4}$$

where $\pi_h \phi$ is some approximation of ϕ in V_h.

REMARK 2.1. *The representation (2.4) is the analog of the Green's function representation of the effect of perturbing the data (1.8). Because we expect $\phi - \pi_h \phi$ to be small and to decrease as the mesh is refined, we see that the sensitivity of the finite element solution with respect to perturbation in the discretization is fundamentally different than the sensitivity of the true solution to general perturbations in the data.*

In practice, we use the error representation formula (2.4) directly for the purpose of computational error estimation. However, for the purpose of understanding the effects of the decay of influence, we manipulate (2.4) to make it more amenable to analysis. We break up the second integral on the right as

$$\int_\Omega \nabla U \cdot \nabla(\phi - \pi_h \phi) \, dx = \sum_{K \in \mathcal{T}_h} \int_K \nabla U \cdot \nabla(\phi - \pi_h \phi) \, dx.$$

Using Green's formula, we have

$$\int_K \nabla U \cdot \nabla(\phi - \pi_h \phi) \, dx = -\int_K \Delta U (\phi - \pi_h \phi) \, dx + \int_{\partial K} \nabla U \cdot n_{\partial K} (\phi - \pi_h \phi) \, ds,$$

where the last term is a line integral and $n_{\partial K}$ denotes the outward normal to ∂K.

Upon summing over all elements $K \in \mathcal{T}_h$, the boundary integrals give two contributions from each element edge, computed in opposite directions. Suppose $K_1, K_2 \in \mathcal{T}_h$ share a common edge $\sigma_1 \subset \partial K_1 = \sigma_2 \subset \partial K_2$. The contribution from that edge is

$$\begin{aligned}
&\int_{\sigma_1} \nabla U|_{K_1} \cdot n_{\sigma_1} (\phi - \pi_h \phi) \, ds + \int_{\sigma_2} \nabla U|_{K_2} \cdot n_{\sigma_2} (\phi - \pi_h \phi) \, ds \\
&\qquad = \int_{\sigma_1} \nabla U|_{K_1} \cdot n_{\sigma_1} (\phi - \pi_h \phi) \, ds - \int_{\sigma_1} \nabla U|_{K_2} \cdot n_{\sigma_1} (\phi - \pi_h \phi) \, ds \\
&\qquad = -\int_{\sigma_1} [\nabla U] \cdot n_{\sigma_1} (\phi - \pi_h \phi) \, ds,
\end{aligned}$$

where $[U] = \nabla U|_{K_2} - \nabla U|_{K_1}$ denotes the "jump" in ∇U across σ_1 in the direction of the normal $n_{\partial K_1}$.

When summing over the elements, we associate half of the common contribution across a shared edge between two elements with each element. We obtain an alternate error representation,

$$\|e\|_{1,\omega} = -\sum_{K\in\mathcal{T}_h}\left(\int_K (\Delta U + f)(\phi - \pi_h\phi)\,dx - \frac{1}{2}\int_{\partial K}[\nabla U]\cdot n_{\partial K}(\phi-\pi_h\phi)\,ds\right).$$

Anticipating the analysis, we define the residual and corresponding dual weights,

$$\mathcal{R}_K = \begin{pmatrix}\|\Delta U + f\|_K \\ \|h^{-1/2}[\nabla U]\|_{\partial K}/2\end{pmatrix},\ \mathcal{W}_K = \begin{pmatrix}\|\phi-\pi_h\phi\|_K \\ \|h^{1/2}(\phi-\pi_h\phi)\|_{\partial K}\end{pmatrix}. \tag{2.5}$$

We obtain an *a posteriori* error bound similar to the results in [8],

THEOREM 2.1. *The energy norm error of the finite element approximation (2.2) on ω is bounded by*

$$\|e\|_{1,\omega} \le \sum_{K\in\mathcal{T}_h}\mathcal{R}_K\cdot\mathcal{W}_K.$$

To understand the effect of the decay of influence, we first note that there is a constant C independent of the mesh such that

$$\mathcal{R}_K \le C|K|^{1/2},$$

where $|K|$ denote the area of $K\in\mathcal{T}_h$. The bound on the first component of $\mathcal{R}_K$ is simple, $\|\Delta U + f\|_K = \|f\|_K \le \max_\Omega|f|\times|K|^{1/2}$. To bound the second component, consider an integral over the common edge σ between two elements K_1 and K_2,

$$\|[\nabla U]\|_\sigma = \|\nabla U|_{K_2} - \nabla U|_{K_1}\|_\sigma \le \|\nabla U|_{K_2} - \nabla u|_\sigma\|_\sigma + \|\nabla u|_\sigma - \nabla U|_{K_1}\|_\sigma.$$

By a trace inequality, the standard energy norm convergence result, and a standard elliptic regularity result, we have

$$\begin{aligned}\|\nabla U|_{K_i} - \nabla u|_\sigma\|_\sigma &\le \|\nabla U - \nabla u\|_{K_i}^{1/2}\|\nabla U - \nabla u\|_{1,K_i}^{1/2} \le C\|hu\|_{2,K_i}^{1/2}\|u\|_{2,K_i}^{1/2}\\ &\le C\|h^{1/2}f\|_{K_i},\end{aligned}$$

for $i=1,2$. The local quasi-uniformity of the mesh implies $\frac{1}{2}\|h^{-1/2}[\nabla U]\|_{\partial K} \le C\max_\Omega|f|\times|K|^{1/2}$.

Therefore, the convergence of the Galerkin approximation is determined primarily by the dual weights $\phi-\pi_h\phi$, i.e. by the approximation properties of V_h and the smoothness of ϕ. If we let $G(x,y)$ denote the Green's function for the Laplacian on Ω, then

$$\phi(x) = \int_\Omega G(x,y)\psi(y)\,dy = \int_\omega G(x,y)\psi(y)\,dy.$$

There are two cases to consider. For $y\in\omega$, $G(x,y)$ is a smooth function of x for $x\in\Omega\setminus\omega$, and therefore so is ϕ. We can compute derivatives via

$$D_x^\alpha\phi(x) = \int_\omega D_x^\alpha G(x,y)\psi(y)\,dy.$$

We assume that $\delta>0$ is small enough that $\omega_\delta = \{x\in\Omega : \operatorname{dist}(x,\omega)\le\delta\}$ is contained in Ω, but large enough that for $K\subset\Omega\setminus\omega_\delta$, the union $\mathcal{N}(K)$ of K and the elements bordering K does not intersect ω. See Fig. 2.1. For $K\subset\Omega\setminus\omega_\delta$, we let π_h be the Lagrange nodal interpolant with respect to $\mathcal{T}_h$, so that

$$\|\phi-\pi_h\phi\|_K \le C\sum_{|\alpha|=2}\|h^2D^\alpha\phi\|_K.$$

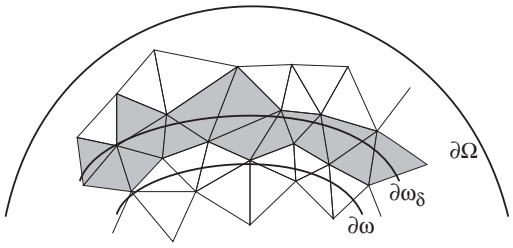

FIG. 2.1. *The choice of* ω_δ.

On the other hand, we cannot expect ϕ to be smoother than H^1 in ω. For $K \cap \omega_\delta \neq \emptyset$, we let π_h be the Scott-Zhang interpolant ([4]), for which we have

$$\|\phi - \pi_h\phi\|_K \leq C|h\phi|_{1,\mathcal{N}(K)},$$

for a mesh-independent constant C.

We have bounded the first component of $\mathcal{W}_K$. The second component is bounded in the same way after first using a trace theorem to obtain,

$$\|h^{1/2}(\phi - \pi_h\phi)\|_{\partial K} \leq \|\phi - \pi_h\phi\|^{1/2}_{\mathcal{N}(K)}\|h(\phi - \pi_h\phi)\|^{1/2}_{1,\mathcal{N}(K)},$$

and then using the local quasi-uniformity of the mesh. We conclude,

THEOREM 2.2. *For any* $\delta > 0$ *small enough that* $\omega_\delta \subset \Omega$ *but large enough that* $\mathcal{N}(K) \cap \omega = \emptyset$ *for* $K \subset \Omega \setminus \omega_\delta$*, there is a constant* C *such that the energy norm error of the finite element approximation (2.2) on* ω *is bounded by*

$$\|e\|_{1,\omega} \leq \sum_{K\subset\Omega\setminus\omega_\delta} \sum_{|\alpha|=2} C\|h^2 D^\alpha\phi\|_K|K|^{1/2} + \sum_{K\cap\omega_\delta\neq\emptyset} C|h\phi|_{1,\mathcal{N}(K)}|K|^{1/2}. \tag{2.6}$$

To understand the implications of (2.6) for mesh selection in an adaptive setting, we further estimate the quantities on the right in (2.6).

To handle the first sum on the right, we estimate the derivatives using the Green's function as

$$\begin{aligned}
\|D_x^\alpha\phi\|_K^2 &= \int_K \left(\int_\omega D_x^\alpha G(x,y)\psi(y)\,dy\right)^2 dx \\
&\leq \int_K \|D_x^\alpha G(x,\cdot)\|^2_{1,\omega}\|\psi\|^2_{-1,\omega}\,dx \\
&= \sum_{|\beta|=1}\int_K\int_\omega |D_x^\alpha D_y^\beta G(x,y)|^2\,dydx + \int_K\int_\omega |D_x^\alpha G(x,y)|^2\,dydx.
\end{aligned}$$

We use *MAPLE*© to expand the necessary derivatives of the formula (1.9) for G as an asymptotic series in $1/|x-y|$. We find that there is a constant C such that

$$|D_x^\alpha D_y^\beta G(x,y)| \leq \frac{C}{|x-y|^2}, \quad x \neq y \in \Omega,\ |\alpha| = 2,\ |\beta| \leq 1.$$

We conclude there is a constant C independent of the mesh such that for $K \subset \Omega \setminus \omega_\delta$,

$$\|\phi - \pi_h\phi\|_K \leq \frac{Ch_K^2}{\text{dist}\,(K,\omega)^2}|K|^{1/2}.$$

To handle the second sum on the right of (2.6), we use the basic stability estimate,

$$\|\phi\|_{1,\Omega} \leq \|\psi\|_{-1,\Omega} = \|\psi\|_{-1,\omega} = 1.$$

If we assume a uniform (small) size $h_K = \underline{h}$ for elements such that $K \cap \omega_\delta \neq \emptyset$, we obtain

$$\sum_{K\cap\omega_\delta\neq\emptyset} Ch_K|\phi|_{1,\mathcal{N}(K)} \leq C\underline{h}\|\phi\|_{1,\Omega} = C\underline{h} = \frac{C}{|\omega_\delta|}\sum_{K\cap\omega_\delta\neq\emptyset}\underline{h}|K|.$$

We conclude

THEOREM 2.3. *For any $\delta > 0$ small enough that $\omega_\delta \subset \Omega$ but large enough that $\mathcal{N}(K)\cap\omega = \emptyset$ for $K \subset \Omega\setminus\omega_\delta$, there is a constant C such that the energy norm error of the finite element approximation (2.2) on ω is bounded by*

$$\|e\|_{1,\omega} \leq \sum_{K\subset\Omega\setminus\omega_\delta} \frac{Ch_K^2}{\operatorname{dist}(K,\omega)^2}|K| + \sum_{K\cap\omega_\delta\neq\emptyset} C\underline{h}|K|. \tag{2.7}$$

In common approaches to adaptive error control, a "Principle of Equidistribution" shows that the element contributions to the error are approximately equal in an nearly optimal mesh. In (2.7), the element indicators are $Ch_K^2/\operatorname{dist}(K,\omega)^2$ respectively $C\underline{h}$. In particular, we conclude that in an optimal adapted mesh,

$$\frac{h_K^2}{\operatorname{dist}(K,\omega)^2} \approx \underline{h} \quad \text{or} \quad h_K \approx \underline{h}^{1/2}\times\operatorname{dist}(K,\omega), \quad K\subset\Omega\setminus\omega_\delta.$$

We can immediately see the effects of the decay of influence inherent to the Laplacian on the disk. Away from the region ω where we estimate the norm, we can choose elements asymptotically larger than the element size used in ω_δ because of the smoothness properties of the Green's function. Moreover, the elements can increase the size as the distance to ω_δ increases because of the decay properties of the Green's function. In this problem, we call ω_δ the effective domain of influence for the error in the energy norm in ω. The effective domain of influence is characterized by the requirement that the mesh size needed for accurate computation is small in the effective domain, but increases away from the effective domain.

3. An a posteriori error analysis using the generalized Green's function. In this section, we explain how the *a posteriori* error analysis presented in Sec. 2 can be extended to more general situations. Again, the analysis follows the ideas introduced in [8] closely. We consider a general second order linear elliptic boundary value problem for a scalar solution,

$$\begin{cases} L(D,x)u(x) = -\nabla\cdot(a(x)\nabla u(x)) + b(x)\cdot\nabla u(x) + c(x)u(x) = f(x), & x\in\Omega, \\ u(x) = 0, & x\in\partial\Omega, \end{cases} \tag{3.1}$$

where $\Omega\subset\mathbb{R}^d$, $d = 2,3$, is a convex, polygonal domain; $a = (a_{ij})$, where $a_{i,j}$ are continuous in the closure $\overline{\Omega}$ for $1\leq i,j\leq n$ and there is a $a_0 > 0$ such that $v^\top a v \geq a_0$ for all $v\in\mathbb{R}^d\setminus\{0\}$ and $x\in\Omega$; $b = (b_i)$ where b_i is continuous in $\overline{\Omega}$; and finally c and f are continuous in $\overline{\Omega}$. Extensions to more general problems and situations are possible, see [12].

We discretize (3.1) by applying a finite element method to the associated variational formulation:

Find $u\in H_0^1(\Omega)$ such that

$$A(u,v) = (a\nabla u,\nabla v) + (b\cdot\nabla u, v) + (cu,v) = (f,v) \text{ for all } v\in H_0^1(\Omega). \tag{3.2}$$

We use the standard continuous, piecewise linear finite element method with respect to a locally quasi-uniform simplex triangulation $\mathcal{T}_h$ of Ω. With the same setup as in Sec. 2, the finite element method is:

$$\text{Compute } U\in V_h \text{ such that } A(U,v) = (f,v) \text{ for all } v\in V_h. \tag{3.3}$$

By standard results, we know that U exists and converges to u as $h\to 0$.

The goal of the *a posteriori* error analysis conducted below is to estimate the error in a quantity of interest computed from the finite element solution U. Consider the example in Sec. 2, where we estimate the energy norm of the error, which is the error in ∇U, in a small region inside Ω. To do this, we use a particular solution ϕ of the adjoint problem corresponding to a special choice of data ψ and use the Green's function for the differential equation to estimate the values of ϕ.

Classical analysis of finite element methods tends to focus on estimating the error in global norms, such as $\| \quad \|_{L^2(\Omega)}$, $\| \quad \|_{L^\infty(\Omega)}$, and of course the energy norm. In practice, however, this may not be meaningful. Often, the practical goal for solving a differential equation is to compute specific information from the solution, and in those situations, we should naturally be concerned with the error in the desired information. This may not have much to do with the error in some global norm. In contrast, the *a posteriori* error analysis presented below allows estimation of the error in information computed from the solution that can be represented as (u, ψ), where ψ is a distribution in $H^{-1}(\Omega)$ for example. Note that some common norms can also be represented in this way.

These considerations also suggest an extension of the classic concept of a Green's function. Traditionally, the Green's function is defined as a particular adjoint solution corresponding to data δ_x in order to obtain the value of the solution $u(x)$. This is motivated on theoretical grounds by the issues of existence and uniqueness of solutions. Moreover, the special properties of the δ distribution make it possible to find an exact formula for the Green's function on some simple domains. But, knowing the point values of the solution may not be very relevant to a practical application of a differential equation. Instead, the natural extension of the Green's function corresponds to the data ψ that gives the desired information of the solution via (u, ψ). Moreover, we do not expect to find a formula for the Green's function for a general operator on complicated domains, removing another reason to restrict to the δ distribution.

Therefore, we assume that the information we wish to compute can be represented as (u, ψ) where $\psi \in H^{-1}(\Omega)$. We define the **generalized Green's function** ϕ as the solution of the weak adjoint problem,

Find $\phi \in H_0^1(\Omega)$ such that

$$A^*(v, \phi) = (\nabla v, a\nabla\phi) - (v, \operatorname{div}(b\phi)) + (v, c\phi) = (v, \psi) \text{ for all } v \in H_0^1(\Omega), \quad (3.4)$$

corresponding to the adjoint problem $L^*(D, x)\phi = \psi$. Arguing as in Sec. 2,

$$\begin{aligned}(e, \psi) &= (\nabla e, a\nabla\phi) - (e, \operatorname{div}(b\phi)) + (e, c\phi)\\ &= (a\nabla e, \nabla\phi) + (b \cdot \nabla e, \phi) + (ce, \phi)\\ &= (a\nabla u, \nabla\phi) + (b \cdot \nabla u, \phi) + (cu, \phi) - (a\nabla U, \nabla\phi) - (b \cdot \nabla U, \phi) - (cU, \phi)\\ &= (f, \phi) - (a\nabla U, \nabla\phi) - (b \cdot \nabla U, \phi) - (cU, \phi).\end{aligned}$$

Letting $\pi_h\phi$ denote an approximation of ϕ in V_h, using Galerkin orthogonality, we conclude

THEOREM 3.1. *The error of the finite element solution (3.3) satisfies the* **error representation**,

$$(e, \psi) = (f, \phi - \pi_h\phi) - (a\nabla U, \nabla(\phi - \pi_h\phi)) - (b \cdot \nabla U, \phi - \pi_h\phi) - (cU, \phi - \pi_h\phi), \quad (3.5)$$

where the generalized Green's function ϕ satisfies the adjoint problem (3.4) corresponding to data ψ.

We can interpret the quantity (e, ψ) as a linear functional of the error. Also, if ψ is suitably normalized, (e, ψ) represents a projection of the error in the direction of ψ. Some useful choices of ψ include:

- To estimate the average error over $\omega \subset \Omega$, we choose $\psi = \chi_\omega/|\omega|$, where χ_ω is the characteristic function of ω. We can similarly obtain weighted averages.
- To obtain the error at a point x, we choose $\psi = \delta_x$. We can obtain the average error on a curve c by choosing $\psi = \delta_c$ in $\mathbb{R}^d$, $d = 2, 3$, and on a plane surface s by choosing $\psi = \delta_s$ in $\mathbb{R}^3$. We can obtain errors in derivatives using dipoles in the same way.

- The error in the $L^2(\omega)$ norm, $\|e\|_\omega$, for some $\omega \subset \Omega$, is theoretically given by $\psi = \chi_\omega e/\|e\|_\omega$. Of course, we cannot simply choose this ψ in practice. However in practice, good approximations can be obtained with Richardson extrapolation using finite element solutions with different accuracy.
- In the case that $b \equiv c \equiv 0$, we can estimate the energy norm $a(e,e)$, by choosing $\psi = \mathcal{R}$, where $\mathcal{R}$ is the residual defined weakly by

$$(\mathcal{R}, v) = (a\nabla U, \nabla v) - (f, v) \text{ for all } v \in H_0^1(\Omega).$$

  This yields $(\mathcal{R}, e) = A(e,e)$ since

$$(\mathcal{R}, e) = (a\nabla U, \nabla e) - (f, e) = (a\nabla U, \nabla e) - (a\nabla u, \nabla e) = (a\nabla e, \nabla e).$$

  In other words, the data ψ yielding the energy norm in the variational definition (2.3) is actually easy to specify. An elementwise expression (2.5) for $\mathcal{R}$ is derived in Sec. 2 in the case that a is the identity.

Note that among these choices, some of the ψ are spatially localized and some are not.

For the purpose of computational error estimation, we use (3.5) directly rather than making further estimates. For one thing, *a priori* estimates on the quantities on the right-hand side of (3.5) tend to lead to gross overestimation, mainly due to reduction of the effects of cancellation of error. For another, we do not expect to have accurate estimates on the adjoint weighting function $\phi - \pi_h\phi$. This is in sharp contrast to the problems considered in [8] and in Sec. 2 above. Instead, we approximate ϕ using a finite element method. Since $\phi - \pi_h\phi \sim \sum_{|\alpha|=2} D^\alpha \phi$ where ϕ is smooth, we use a higher order finite element than that used to solve the original boundary value problem (3.1). For example, good results are obtained using the space V_h^2 of continuous, piecewise quadratic functions with respect to $\mathcal{T}_h$. The approximate generalized Green's function is

Compute $\Phi \in V_h^2$ such that

$$A^*(v, \Phi) = (\nabla v, a\nabla\Phi) - (v, \operatorname{div}(b\Phi)) + (v, c\Phi) = (v, \psi) \text{ for all } v \in V_h^2. \quad (3.6)$$

The corresponding **approximate error representation** is

$$(e, \psi) \approx (f, \Phi - \pi_h\Phi) - (a\nabla U, \nabla(\Phi - \pi_h\Phi)) - (b \cdot \nabla U, \Phi - \pi_h\Phi) - (cU, \Phi - \pi_h\Phi). \quad (3.7)$$

REMARK 3.1. *This approach to a posteriori error analysis was introduced in [8]. The idea of using a numerical approximation of the generalized Green's function in conjunction with the error estimate was introduced experimentally in [5] and fully developed in the context of ordinary differential equations in [9]. In contrast, the early analysis of partial differential equations in [8] concentrated on problems for which accurate* a priori *estimates on the adjoint weights are possible. Since these early contributions, there has been much progress made on this approach by various groups, see [6, 13, 3, 15] . The use of an approximate generalized Green's function raises many questions regarding convergence, reliability, and accuracy. Addressing these here would lead too far astray, so we refer to [13, 12] for such details. We simply note in practice that astoundingly accurate and reliable results are obtained using this approach, see [11] for example. The cost is of course the need to solve the adjoint problem.*

For the purpose of implementing (3.7) to obtain a computational error estimate and for adaptive error control, we rewrite it as a sum of element contributions,

$$(e, \psi) \approx \sum_{K \in \mathcal{T}_h} \int_K \big((f - b \cdot \nabla U - cU)(\Phi - \pi_h\Phi) - a\nabla U \cdot \nabla(\Phi - \pi_h\Phi)\big)\, dx. \quad (3.8)$$

Each of the integrals on the right-hand side are typically evaluated using a high order quadrature method.

As in Sec. 2, we define the notion of an effective domain of influence through consideration of adaptive meshing. A typical goal of adaptive error control is to find a mesh with a relatively small number of elements such that for a given tolerance TOL and data ψ,

$$|(e,\psi)| \leq \text{TOL}.$$

We use (3.8) to replace this with the practical goal of satisfying the **mesh acceptance criterion**:

$$\left| \sum_{K\in\mathcal{T}_h} \int_K \big((f - b\cdot\nabla U - cU)(\Phi - \pi_h\Phi) - a\nabla U\cdot\nabla(\Phi-\pi_h\Phi)\big)\,dx \right| \leq \text{TOL}. \tag{3.9}$$

In order to apply the standard variational "Principle of Equidistribution" argument, we require an estimate consisting of a sum over elements of positive quantities. Thus, if (3.9) is **not** satisfied, then the mesh is refined in order to achieve the more conservative condition,

$$\sum_{K\in\mathcal{T}_h} \int_K \big|(f - b\cdot\nabla U - cU)(\Phi - \pi_h\Phi) - a\nabla U\cdot\nabla(\Phi-\pi_h\Phi)\big|\,dx \leq \text{TOL}. \tag{3.10}$$

Then, the element indicators on a nearly optimal mesh are roughly equal across the elements. Depending on the argument, we may use

$$\max_K \big|(f - b\cdot\nabla U - cU)(\Phi - \pi_h\Phi) - a\nabla U\cdot\nabla(\Phi-\pi_h\Phi)\big| \lesssim \frac{\text{TOL}}{|\Omega|}, \tag{3.11}$$

or

$$\int_K \big|(f - b\cdot\nabla U - cU)(\Phi - \pi_h\Phi) - a\nabla U\cdot\nabla(\Phi-\pi_h\Phi)\big|\,dx \lesssim \frac{\text{TOL}}{M}, \tag{3.12}$$

as **element acceptance criteria**, where M is the number of elements in $\mathcal{T}_h$. Computing a mesh using these criteria is usually performed by a "compute-estimate-mark-refine" adaptive strategy that begins with a coarse mesh and then refines those elements on which (3.11) respectively (3.12) fail successively.

An **effective domain of influence** corresponding to the data ψ for the generalized Green's function is the region in which the corresponding elements **must** be significantly smaller in size than the elements used in the complement $\Omega\setminus\omega_\psi$ in order to satisfy (3.9). Equivalently, if $\mathcal{T}_h$ comprises uniformly sized elements, then the effective domain of influence comprises those elements on which the element indicators (3.11), alternatively (3.12), are substantially larger than those in the complement.

Doubtless, this is a vague notion since it depends on the coarseness of the initial mesh in the adaptive process, the procedure of mesh refinement, and the "border" regions between areas of highly refined elements and areas of coarse meshes. Nevertheless, we demonstrate that it is still a useful idea in certain circumstances. The effective domain of influence ω_ψ is especially useful when it comprises a relatively small part of Ω, in which case adaptive mesh refinement can be used to significant advantage.

4. A decomposition of the solution. In Sec. 3, we derived an estimate for the error in one piece of information (U,ψ) computed from a finite element solution U, where ψ is a given distribution. In practice, it is often the case that the goal is to compute several kinds of information. For example, we might wish to compute values of the solution at a certain number of points and internal boundaries. In this section, we explain how the problem of computing multiple quantities of interest also arises naturally when the data ψ for the adjoint problem does not have spatially localized support. Examples include estimating the error in a weighted average or norm over the domain Ω.

We are motivated by the observation that the cases where there is an exact formula for the Green's function suggest that there will not be a significant effect from the decay of influence

when the support of the data for the adjoint problem is not spatially localized. Certainly, if the data ψ has the property that the corresponding adjoint weight $\phi - \pi_h \phi$ has a more-or-less uniform size throughout Ω, then the degree of non-uniformity in an adapted mesh depends largely on the spatial variation of the residual.

However, we can use a partition of unity to "localize" a problem in which $\mathrm{supp}\,(\psi)$ does not have local support. We let $\{\Omega_i\}_{i=1}^N$ be a finite open cover of Ω. A **Lipschitz partition of unity** subordinate to $\{\Omega_i\}$ is a collection of functions $\{p_i\}_{i=1}^N$ with the properties that p_i is continuous on Ω and differentiable on Ω_i for $1 \le i \le N$ and moreover

$$\mathrm{supp}\,(p_i) \subset \overline{\Omega}_i, \quad 1 \le i \le N, \tag{4.1}$$

$$\sum_{i=1}^N p_i(x) = 1, \quad x \in \Omega, \tag{4.2}$$

$$\|p_i\|_{L^\infty(\Omega)} \le C \text{ and } \|\nabla p_i\|_{L^\infty(\Omega_i)} \le C/\mathrm{diam}\,(\Omega_i), \quad 1 \le i \le N, \tag{4.3}$$

where C is a constant and $\mathrm{diam}\,(\Omega_i)$ is the diameter of Ω_i.

Several partitions of unity satisfying (4.1)-(4.3) exist. In the case of a polygonal domain Ω, the simplest construction employs continuous piecewise linear finite element basis functions defined on a simplex mesh subdivision $\mathcal{S}$ of Ω. The $\{\Omega_i\}$ are built by first constructing a disjoint partition $\{\Omega_i^\circ\}$ of $\mathcal{S}$ using e.g. spectral or inertial bisection [2]. Each of the disjoint Ω_i° are extended to define Ω_i by considering all boundary vertices of Ω_i°; all simplices of neighboring Ω_j°, $j \ne i$ which are contained in the boundary vertex 1-rings of Ω_i° are added to Ω_i° to form Ω_i. This procedure produces the smallest overlap for the $\{\Omega_i\}$, such that the properties (4.1)–(4.3) are satisfied by the resulting $\{\phi_i\}$ built from the nodal continuous piecewise linear finite element basis functions. More sophisticated constructions with superior properties are possible; see e.g. [16].

Now we use a partition of unity $\{p_i\}$ to write $\psi \equiv \sum_{i=1}^N \psi p_i$ and consider the problem of estimating the error in the localized information $(U, \psi p_i)$ corresponding to data $\psi_i = \psi p_i$ for some $1 \le i \le N$. Correspondingly, we obtain a finite element solution via:

$$\text{Compute } \hat{U}_i \in \hat{V}_i \text{ such that } A(\hat{U}_i, v) = (f, v) \text{ for all } v \in \hat{V}_i, \tag{4.4}$$

where $\hat{V}_i$ is a space of continuous, piecewise linear functions on a locally quasi-uniform simplex triangulation $\mathcal{T}_i$ of Ω obtained by (presumably local) refinement of an initial coarse triangulation $\mathcal{T}_0$ of Ω. We emphasize that the spaces $\{\hat{V}_i\}$ are globally defined and the "localized" problems (4.4) are solved over the entire domain. The hope is that these problems will require localized mesh refinements because the corresponding data has localized support.

We can obtain a partition of unity approximation in the sense of Babuška and Melenk [1] by defining the truly local approximations $U_i = \chi_i \hat{U}_i$, $1 \le i \le N$, where χ_i is the characteristic function of Ω_i. The local approximation U_i is in the local finite element space $V_i = \chi_i \hat{V}_i$. The **partition of unity approximation** is defined by

$$U_p = \sum_{i=1}^N U_i p_i,$$

which is in the **partition of unity finite element space**

$$V_p = \sum_{i=1}^N V_i p_i = \left\{ \sum_{i=1}^N v_i p_i : v_i \in V_i \right\}.$$

The basic convergence results for this method are proved in [17] and [18] using ideas of Babuška and Melenk [1] and Xu and Zhou [21]. The upshot is that the partition of unity approximation recovers the full convergence properties of an approximation of the original solution. Note that

$$U_p = \sum_{i=1}^N U_i p_i = \sum_{i=1}^N \chi_i \hat{U}_i p_i \equiv \sum_{i=1}^N \hat{U}_i p_i.$$

In words, the values of U_i or $\hat{U}_i$ outside of Ω_i are immaterial in forming the global partition of unity approximation.

To estimate the error in the localized information corresponding to ψ_i, we use the generalized Green's function satisfying the adjoint problem:

$$\text{Find } \phi_i \in H_0^1(\Omega) \text{ such that } A^*(v,\phi_i) = (v,\psi_i) \text{ for all } v \in H_0^1(\Omega). \tag{4.5}$$

We expand the global error in the partition of unity approximation as

$$(u - U_p, \psi) = \sum_{i=1}^{N} \big((u - U_i)p_i, \psi\big).$$

We estimate each summand on the right as

$$\begin{aligned}\big((u - U_i)p_i, \psi\big) &= (u - \hat{U}_i, \psi_i) = A^*(u - \hat{U}_i, \phi_i) \\ &= (f,\phi_i) - (a\nabla\hat{U}_i, \nabla\phi_i) - (b\cdot\nabla\hat{U}_i, \phi_i) - (c\hat{U}_i, \phi_i).\end{aligned}$$

Letting $\pi_i\phi_i$ denote an approximation of ϕ_i in $\hat{V}_i$, using Galerkin orthogonality, we conclude

THEOREM 4.1. *The error of the partition of unity finite element solution U_p satisfies the error representation,*

$$\begin{aligned}&(u - U_p, \psi) \\ &\qquad = \sum_{i=1}^{N} \big((f, \phi_i - \pi_i\phi_i) - (a\nabla\hat{U}_i, \nabla(\phi_i - \pi_i\phi_i)) - (b\cdot\nabla\hat{U}_i, \phi_i - \pi_i\phi_i) \\ &\qquad\qquad - (c\hat{U}_i, \phi_i - \pi_i\phi_i)\big), \end{aligned} \tag{4.6}$$

where ϕ_i is the solution of the adjoint problem (4.5) and $\hat{U}_i$ solves the finite element problem (4.4) corresponding to the localized data ψ_i.

In practice, we compute approximate generalized Green's functions via;

$$\text{Compute } \Phi_i \in V_i^2 \text{ such that } A^*(v,\Phi_i) = (v,\psi_i) \text{ for all } v \in V_i^2, \quad 1 \le i \le N, \tag{4.7}$$

where V_i^2 is the space of continuous, piecewise quadratic functions with respect to $\mathcal{T}_i$. The corresponding approximate error representation for each computation is

$$\begin{aligned}&(u - \hat{U}_i, \psi_i) \\ &\qquad \approx (f, \Phi_i - \pi_i\Phi_i) - (a\nabla\hat{U}_i, \nabla(\Phi_i - \pi_i\Phi_i)) - (b\cdot\nabla\hat{U}_i, \Phi_i - \pi_i\Phi_i) \\ &\qquad\qquad - (c\hat{U}_i, \Phi_i - \pi_i\Phi_i). \end{aligned} \tag{4.8}$$

Note that the proof of Theorem 4.1 also implies that if the localized error satisfies

$$\big|(u - \hat{U}_i, \psi_i)\big| \le \frac{\text{TOL}}{N}, \quad 1 \le i \le N, \tag{4.9}$$

then $|(u - U_p, \psi)| \le \text{TOL}$. This justifies treating the N "localized" problems independently in terms of mesh refinement.

5. Efficient computation of multiple quantities of interest using the effective domain of influence. In this section, we develop an algorithm for computing multiple quantities of interest from the solution of an elliptic problem efficiently using knowledge of the effective domains of influence of the corresponding Green's functions. We assume that the information is specified as $\{(U,\psi_i)\}_{i=1}^N$ for a set of N functions $\{\psi_i\}_{i=1}^N$. These data might arise as particular goals or via localization through a partition of unity. We assume that the goal is to compute the information associated to ψ_i so that the error is smaller than a tolerance TOL_i for $1 \le i \le N$.

There are two approaches for this problem that lie at the opposite ends of a range of possibilities:

Approach 1: **A Global Computation**
Find one triangulation such that the corresponding finite element solution satisfies

$$|(e, \psi_i)| \leq \text{TOL}_i, \quad 1 \leq i \leq N.$$

This is implemented with a straightforward modification of the standard adaptive strategy in which the N mesh acceptance criteria corresponding to the N data are checked on each element and if any of the N criteria fail, the element is marked for refinement.
Approach 2: **A Decomposed Computation**
Find N independent triangulations and finite element solutions U_i so that the errors satisfy

$$|(e_i, \psi_i)| \leq \text{TOL}_i, \quad 1 \leq i \leq N.$$

Generally, if the correlation, i.e., overlap, between the effective domains of influence associated to the N data $\{\psi_i\}$ is relatively small and the effective domains of influence are relatively small subsets of Ω, then each individual solution in the Decomposed Computation will require significantly fewer elements than solution in the Global Computation to achieve the desired accuracy. This can yield significant computational advantage in terms of lowering the maximum memory requirement to solve the problem or in terms of coarse-grained parallelization when the N computations in the Decomposed Computation can be carried out simultaneously. We provide some examples showing the possible gain in Sec. 7. Vice versa, if the effective domains of influence associated to the N data $\{\psi\}$ have relatively large intersections, then the individual solutions in the Decomposed Computation will require roughly the same number of elements as the solution for the Global Computation. In this case, there is little to be gained in using the Decomposed Computation.

In general, we can expect that some of the N effective domains of influence associated to data $\{\psi_i\}$ in the Decomposed Computation will correlate significantly and the rest will have low correlation. We can optimize the use of resources by combining computations for data whose associated domains of influence have significant correlation and treating the rest independently. We illustrate this idea in Fig. 5.1.

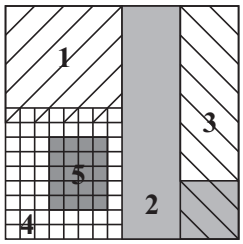

FIG. 5.1. *Decomposing the solution process according to the correlation in the effective domain of influences for multiple data. The shaded regions show the effective domains of influence associated to five data* $\{\psi_1, \cdots, \psi_5\}$. *To optimize computational resources, we solve for four solutions, with one solution aimed at computing the information associated to both* ψ_4 *and* ψ_5. *Note that representing the effective domains as polygonal regions is not unrealistic since typically the effective domains will be described in terms of a triangulation of* Ω.

An algorithm for the decomposition of the solution process using effective domains of influence is:

ALGORITHM 5.1. **Determining the Solution Decomposition**

1. *Discretize* Ω *by an initial coarse triangulation* $\mathcal{T}_0$ *and compute an initial finite element solution* U_0.
2. *Estimate the error in each quantity* (U_0, ψ_i) *by solving the* N *approximate adjoint problems (4.7) and then using (4.8).*
3. *Using the element indicators associated to (4.8) to identify the effective domains of influence for the data* $\{\psi_i\}$ *in terms of the mesh* $\mathcal{T}_0$ *and significant correlations between the effective domains of influence.*

4. *Decide on the number of approximate solutions to be computed and the subset of information to be computed from each solution.*
5. *Compute the approximate solutions independently using adaptive error control aimed at computing the specified quantity or quantities of interest accurately.*

We address the key step 3. in the practical implementation of this algorithm in Sec. 6.

REMARK 5.2. *It is instructive to compare this decomposition of the solution with more traditional domain decomposition. As the name implies, the traditional domain decomposition is a decomposition of the spatial domain. The spatial domain is partitioned into compactly-shaped sub-domains on which approximate problems that are completely local to the sub-domains are solved. Because the solution of the global problem generally involves transmission of information across the entire domain, approximating the global solution by local decomposition solutions involves iterations consisting of alternately passing information, e.g., through boundary conditions, between the sub-domains coupled with solving the localized problems.*

In contrast, the decomposition proposed here is a decomposition of the solution operator associated to the differential equation, not of the domain. The localized problems are solved on the entire domain, though we find this decomposition particularly useful when the mesh nodes are concentrated in relatively small sub-domains of the entire domain. In traditional domain decomposition, any computational savings comes from solving problems that are truly localized. In the proposed approach, any savings comes from the use of coarse discretizations in a major part of the domain. It is important to note that effective domains of influence need not be compactly-shaped. We illustrate this in Example 4 in Sec. 7.

6. Identifying significant correlations between effective domain of influences. The key issue in implementing Algorithm 5.1 is identifying the effective domains of influence for the various generalized Green's functions and recognizing significant correlation, or overlap, between different effective domains of influence in Step 3. In this section, we present a method to do this.

Recall from Sec. 3 that the mesh refinement decisions are based on the sizes of the element indicators on element K,

$$\mathcal{E}_i|_K = \max_K \left|(f - b\cdot\nabla\hat{U}_i - c\hat{U}_i)(\Phi_i - \pi_i\Phi_i) - a\nabla\hat{U}_i\cdot\nabla(\Phi_i - \pi_i\Phi_i)\right| \tag{6.1}$$

or

$$\mathcal{E}_i|_K = \int_K \left|(f - b\cdot\nabla\hat{U}_i - c\hat{U}_i)(\Phi_i - \pi_i\Phi_i) - a\nabla\hat{U}_i\cdot\nabla(\Phi_i - \pi_i\Phi_i)\right| dx, \tag{6.2}$$

associated to the estimate (4.8). We let $\mathcal{E}_i(x)$ denote the piecewise constant element error indicator function associated to data ψ_i with $\mathcal{E}_i(x) \equiv \mathcal{E}_i|_K$ for $K \in \mathcal{T}_0$.

Identifying the effective domain of influence associated to a data means finding a set of elements on which the element error indicators are significantly larger than on the complement, if such a dichotomy exists. Identifying significant correlation between the effective domains of influence of two data entails showing that the effective domains of influence have a significant number of elements in common.

To do this, we borrow a technique from pattern matching in signal processing. Pattern matching is a well-studied problem with applications in a number of areas including template matching and feature detection in image processing applications, and object tracking and target recognition systems in military applications. The foundation of the common algorithms in pattern matching rest on the convolution and correlation.

Of particular importance for the problem at hand is the **(cross-)correlation** of two functions $f \in L^p(\Omega)$ and $g \in L^q(\Omega)$, defined as:

$$(f \circ g)(u) = \int_\Omega f(x)g(u+x)\,dx,$$

which is an $L^1(\Omega)$ function. The correlation function can be interpreted as sliding g by f and computing the overlap inner-product for a given displacement u. In template matching algorithms

used in image and signal processing, the correlations between an input signal and a library of signals are computed and the closest match from the library is the signal containing the "largest" correlation function in some measure. Since each correlation function is itself a real-valued function of n variables, determining the goodness of a match requires computing some real-valued **correlation indicator** $c(f, g)$ of the correlation function $(f \circ g)$, typically an L^p-norm (often the L^∞-norm). The correlation indicator corresponding to each input and library signal pair must be computed and the pair giving the largest value of $c(f, g)$ is taken as the best match.

For the problem of recognizing correlation between effective domains of influence, we treat the element error indicator functions $\{\mathcal{E}_i\}$ as signal functions. In this case, if one signal matches the other signal only after a translation or rotation, we do not consider the functions to be well correlated since this coincides with two primarily disjoint effective domains of influence. Without translation or rotation, correlation of $\mathcal{E}_i$ and $\mathcal{E}_j$ reduces to the L^2-inner-product:

$$(\mathcal{E}_i \circ \mathcal{E}_j)(0) = \int_\Omega \mathcal{E}_i(x)\mathcal{E}_j(x)\,dx = (\mathcal{E}_i, \mathcal{E}_j)_\Omega.$$

The correlation function evaluated at $u = 0$ is just a real number, so that the correlation indicator $c(\mathcal{E}_i, \mathcal{E}_j)$ can be taken as

$$c(\mathcal{E}_i, \mathcal{E}_j) = |(\mathcal{E}_i \circ \mathcal{E}_j)(0)| = (\mathcal{E}_i, \mathcal{E}_j)_\Omega.$$

Note that since the functions $\{\mathcal{E}_i\}$ are all nonnegative, $c(\mathcal{E}_i, \mathcal{E}_j)$ coincides with the L^1-norm of the product function $\mathcal{E}_i\mathcal{E}_j$.

We mark the effective domain of influence associated to ψ_i as significantly correlated to the domain of influence associated to ψ_j if two conditions hold:

1. The correlation of $\mathcal{E}_i$ and $\mathcal{E}_j$ is larger than a fixed fraction of the norm of $\mathcal{E}_j$, or mathematically,

$$c(\mathcal{E}_i, \mathcal{E}_j) \geq \gamma_1 \|\mathcal{E}_j\|_\Omega^2, \tag{6.3}$$

for some fixed $0 \leq \gamma_1 \leq 1$. This essentially means that the projection of $\mathcal{E}_i$ onto $\mathcal{E}_j$ is sufficiently large. We illustrate some typical examples of substantial correlation in Fig. 6.1.

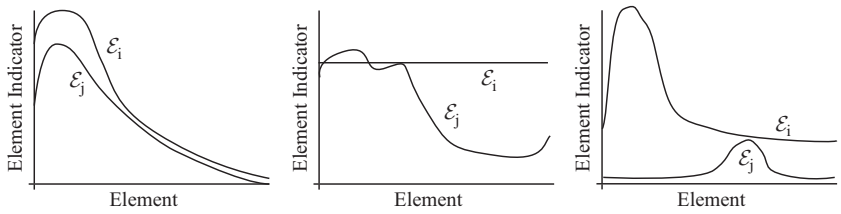

FIG. 6.1. *Three examples of significant correlation of $\mathcal{E}_i$ with $\mathcal{E}_j$. Plotted are the element indicator functions $\mathcal{E}_i(x), \mathcal{E}_j(x)$ versus the element number.*

2. The component of $\mathcal{E}_j$ orthogonal to $\mathcal{E}_i$ is smaller than a fixed fraction of the norm of $\mathcal{E}_j$, or mathematically,

$$\left\| \mathcal{E}_j - \frac{\mathcal{E}_j \circ \mathcal{E}_i}{\|\mathcal{E}_i\|^2} \mathcal{E}_i \right\| \leq \gamma_2 \|\mathcal{E}_j\|, \tag{6.4}$$

for some fixed $0 \leq \gamma_2 \leq 1$. This corrects for the potential difficulties that arise when $\mathcal{E}_i$ is much larger than $\mathcal{E}_j$, leading to significant error in the effective domain of influence corresponding to $\mathcal{E}_j$ possibly being ignored by an adaptive meshing algorithm if the corresponding computations are combined.

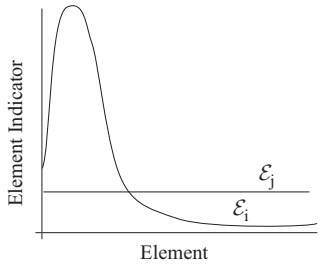

FIG. 6.2. *An example in which condition 2 fails. Plotted are the element indicator functions $\mathcal{E}_i(x), \mathcal{E}_j(x)$ versus the element number.*

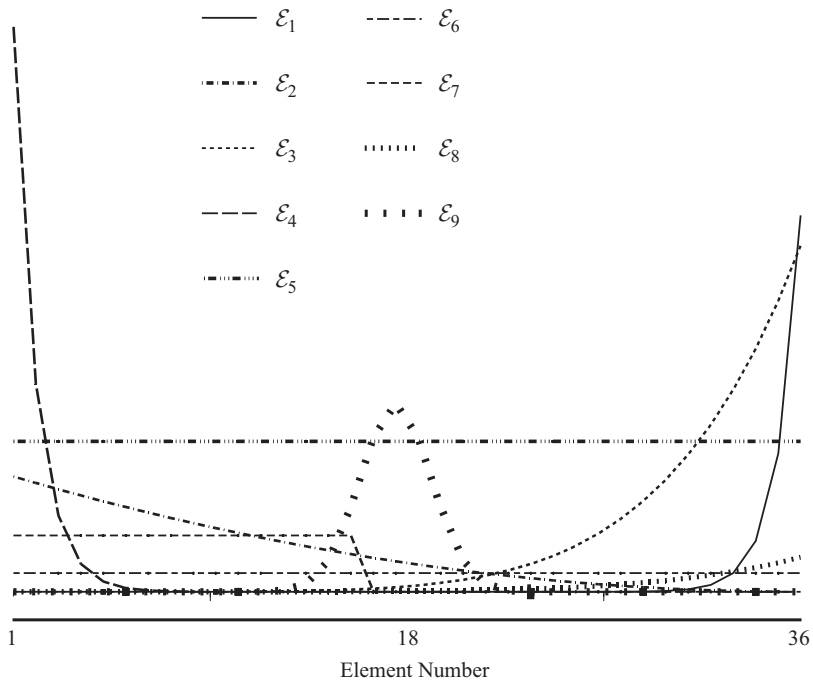

FIG. 6.3. *Plots of nine element indicator functions $\mathcal{E}_i$ versus the element number. Note that in practice, we can not expect plots of the element indicator functions to appear smooth due to the vagaries in ordering when numbering the elements in a triangulation.*

Note that this notion of correlation is not symmetric in $\mathcal{E}_i$ and $\mathcal{E}_j$ as a consequence of the potential differences in size. The examples in Fig. 6.1 makes it clear that symmetry cannot be expected in general.

In Fig. 6.3, we plot a number of element indicator functions $\{\mathcal{E}_i\}$ versus the element number. Applying conditions 1 and 2 with $\gamma_1 = .9$ and $\gamma_2 = .7$ yields the significant correlations:

$\mathcal{E}_1$ with $\mathcal{E}_8$	$\mathcal{E}_4$ with none	$\mathcal{E}_7$ with none
$\mathcal{E}_2$ with $\mathcal{E}_6, \mathcal{E}_7$	$\mathcal{E}_5$ with $\mathcal{E}_2, \mathcal{E}_6$	$\mathcal{E}_8$ with none
$\mathcal{E}_3$ with $\mathcal{E}_1, \mathcal{E}_8$	$\mathcal{E}_6$ with none	$\mathcal{E}_9$ with none

REMARK 6.1. *We emphasize that the initial identification of significant correlation between effective domains of influence of various Green's functions in a computation is carried out on a coarse initial partition of the domain. In general, there is an effective upper limit on the number of partitions in terms of seeing a significant effect from the decay of influence. If the partitions are too dense, then the effective domains of influence will correlate to a significant degree.*

7. Computational examples. In this section, we present several computational examples illustrating and testing the ideas in this paper. In these experiments, we solve various elliptic problems using adaptive mesh refinement to achieve a specified accuracy in a specified set of quantities of interest in two ways. We first use a Global Computation as in Approach 1 described in Sec. 5 and then we use a Decomposed Computation as in Approach 2 implemented using Algorithm 5.1. The results suggest that the individual solutions in the Decomposed Computation require significantly fewer elements to achieve the desired accuracy than the Global Computation because of the decay of influence in a variety of situations.

A significant decrease in the maximum number of elements required to achieve a desired accuracy is important in at least two cases:

1. *Coarse-Grained Parallelization* If the individual solutions in the Decomposed Computation are computed in parallel, then the time needed for the Decomposed Computation is determined roughly by the time it takes to solve for the solution requiring the largest number of elements. If the individual solutions in the Decomposed Computation require significantly fewer elements than the Global Computation, we can expect to see significant speedup.
2. *Computing in a Memory-Constrained Environment* If we are solving in an environment with limited memory capabilities, then decomposing a Global Computation requiring a large number of elements into a set of significantly smaller computations can greatly increase the accuracy of the solution that can be computed and/or decrease the time of solution. In this case, the individual solutions in the Decomposed Computation are computed serially.

Recording the number of elements required to achieve a desired accuracy in specified quantities of interest is easy. Determining the overall gain in efficiency or capability due to reducing the number of elements to achieve a desired accuracy is difficult. In general, the principle factors determining the time it takes for a solution to be computed, including the solution of the nonlinear system determining the approximation, the marking and refinement of meshes in each refinement level, and, in a massively parallel setting, the IO of the data, all scale super-linearly with the number of elements. Moreover, these factors depend heavily on the algorithm, implementation, and machine. So, as a relatively universal measure of the gain from using the Decomposed Computation, we report the Final Element Ratio of the number of elements in the final mesh refinement level required to achieve the specified accuracy in the specified quantities of interest in the Global Computation to the maximum number of elements in the final mesh refinement levels for the individual computations in the Decomposed Computation. Roughly speaking, we can expect the gain in efficiency to scale super-linearly with the Final Element Ratio.

We compute the Final Element Ratio using solutions that are have roughly the same accuracy. In some cases, this may mean adjusting the tolerance and/or the number of elements in the initial mesh in order to achieve the desired accuracy. Generally, the actual error of solutions depends smoothly on the number of elements, but since we do not un-refine elements, the number of elements does not vary smoothly with the tolerance. So, it is better to compare solutions of approximately the same accuracy rather than solutions computed with the same tolerance.

REMARK 7.1. *All computations are performed using* FETkLab *[10]. This adaptive finite element code, running under* MATLAB*, can solve general nonlinear elliptic systems on general domains in two space dimensions. It implements the* a posteriori *error estimate described in Sec. 3 using continuous, piecewise linear elements to solve the original problem and continuous, piecewise quadratic elements on the same mesh to solve adjoint problems for generalized Green's functions.* FEtkLab *allows up to* 16 *simultaneous adjoint data ψ_i to be specified, with some common types of data preprogrammed. There are a number of parameters governing the error estimation and adaptive error control that can be adjusted by the user. In the computations below, we use quadrisection to refine elements. To reduce over-refinement, we limit the number of elements that can be refined in a given refinement level by refining only those indicated elements whose element indicators are larger than the mean plus one standard deviation of all of the element indicators in each refinement level.*

7.1. Example 1. In the first example, we test the partition of unity decomposition of a solution aimed at computing information corresponding to data with global support. We approximate u satisfying the Poisson problem with smooth data,

$$\begin{cases} -\frac{1}{10\pi^2}\Delta u(x) = \sin(\pi x)\sin(\pi y), & (x,y) \in \Omega, \\ u(x,y) = 0, & (x,y) \in \partial\Omega, \end{cases} \tag{7.1}$$

on the domain $\Omega = [0,8] \times [0,8]$. The solution is $u(x,y) = 5\sin(\pi x)\sin(\pi y)$. We solve this problem with the goal of controlling the error in the average value of u by choosing $\psi \equiv 1/|\Omega| = 1/64$.

For the Global Computation, we adapt the mesh so that the error in the average value of u is smaller than the error tolerance of 5%. We begin with an initial mesh of 10×10 elements. After five refinement levels, we end up with 3505 elements, achieving an error of .022. We plot both the initial and final meshes in Fig. 7.1. We plot the numerical solution on the final mesh in Fig. 7.2.

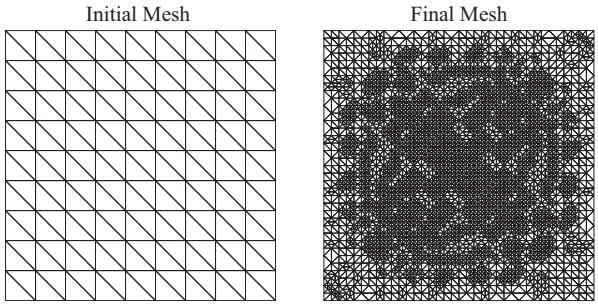

FIG. 7.1. *Initial and final meshes for Example 1 with data ψ giving the average error.*

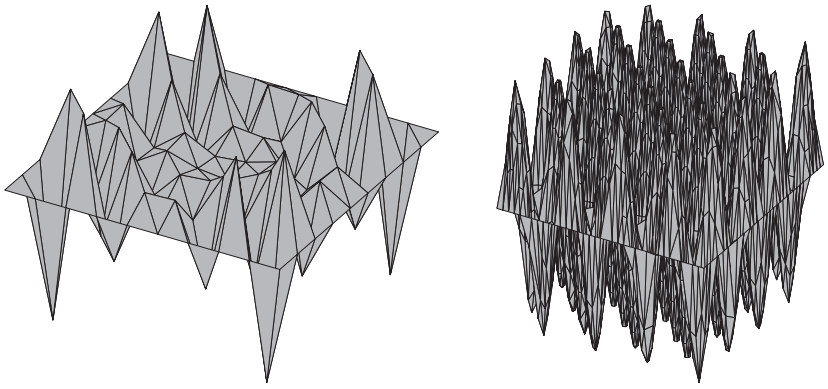

FIG. 7.2. *Numerical solutions on the initial (left) and final (right) meshes for Example 1 with data ψ giving the average error.*

Since we know the true solution, we can compute the actual average error and so evaluate the accuracy of the estimate. Below, we list the estimates, errors, and error/estimate ratios:

Level	Elements	Estimate	Error	Ratio
1	100	.1567	.1534	.9786
2	211	.1157	.1224	1.058
3	585	.3063	.3078	1.005
4	1309	.1159	.1166	1.006
5	3505	.02163	.02148	.9975

We see the excellent accuracy of the computed error estimate at all levels of mesh refinement.

REMARK 7.2. *For the sake of comparison, we present results for the estimation of the $L^2(\Omega)$ norm of the error. This is possible in this example because the error is known. Hence, we can choose $\psi = e/\|e\|_\Omega$ to get $(e,\psi) = \|e\|_\Omega$. We start the computation with the same 10×10 mesh used above, however we use a tolerance of 1% in order to get five refinement levels with the number*

of elements in each refinement level comparable to those used in the computation for the average error. The results are:

Level	*Elements*	*Estimate*	*Error*	*Ratio*
1	100	12.89	19.19	1.488
2	245	13.36	16.21	1.213
3	681	7.120	7.905	1.110
4	1281	4.729	4.830	1.021
5	3267	1.929	2.008	1.041

Again, the results are rather impressive.

In the rest of the examples, we use average error as a globally-defined goal for estimation. We do this to make it easier to compare results from different examples. We do not have the true error available in some of the examples, and estimating the L^2 norm of the error raises significant issues regarding approximation of the dual data. In the tests we conducted on examples in which the error is known, using the average error and the L^2 norm of the error as globally-defined goals produces the same qualitative results.

The data $\psi \equiv 1/64$ is a natural candidate for localization using a partition of unity. We begin with a partition with the four domains shown in Fig. 7.3. Introducing the corresponding partition

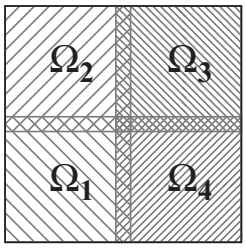

FIG. 7.3. *Domains for the first partition of unity used in Example 1.*

of unity yields four data $\{\psi_1, \psi_2, \psi_3, \psi_4\}$ corresponding to the regions indicated in Fig. 7.3.

REMARK 7.3. *We construct the partition of unity functions by taking the product of independent functions in x and y with the same profile. These functions separate regions of values* 1 *and* 0 *by transition regions $[c-\delta, c+\delta]$ where c is the location of a boundary of the subdomain and δ is a small parameter. In the transition region, we use the monotone function*

$$f(s) = \frac{1}{4\delta^3}\big((s-c)^3 - 3\delta^2(s-c) + 2\delta^3\big), \quad c-\delta \le s \le c+\delta,$$

to transition from 1 *to* 0 *and*

$$f(s) = \frac{1}{4\delta^3}\big((-s+c)^3 - 3\delta^2(-s+c) + 2\delta^3\big), \quad c-\delta \le s \le c+\delta,$$

to transition from 0 *to* 1.

In the first Decomposed Computation, we compute the four localized approximations $\{\hat{U}_1, \cdots, \hat{U}_4\}$ using the same initial mesh as shown in Fig. 7.1. To determine significant correlations, we compute the Correlation Ratios defined as

$$\text{Correlation Ratio 1} = \frac{c(\mathcal{E}_i, \mathcal{E}_j)}{\|\mathcal{E}_j\|_\Omega^2} \quad \text{and} \quad \text{Correlation Ratio 2} = \frac{\left\| \mathcal{E}_j - \dfrac{\mathcal{E}_j \circ \mathcal{E}_i}{\|\mathcal{E}_i\|^2}\mathcal{E}_i \right\|}{\|\mathcal{E}_j\|},$$

where $\{\mathcal{E}_i\}$ are the element indicators. The results are:

Correlation Ratio 1

	$\mathcal{E}_1$	$\mathcal{E}_2$	$\mathcal{E}_3$	$\mathcal{E}_4$
$\mathcal{E}_1\|$	1	.53	.48	.53
$\mathcal{E}_2\|$	1.14	1	1.14	.86
$\mathcal{E}_3\|$	.48	.53	1	.53
$\mathcal{E}_4\|$	1.14	.86	1.14	1

Correlation Ratio 2

	$\mathcal{E}_1$	$\mathcal{E}_2$	$\mathcal{E}_3$	$\mathcal{E}_4$
$\mathcal{E}_1\|$	10^{-16}	.63	.86	.63
$\mathcal{E}_2\|$	.62	10^{-16}	.63	.51
$\mathcal{E}_3\|$	.88	.63	10^{-16}	.63
$\mathcal{E}_4\|$	.62	.51	.63	0

Using $\gamma_1 = .9$ and $\gamma_2 = .5$, this indicates that all four localized solutions should be computed independently.

REMARK 7.4. *An important issue for implementing the Decomposed Computation when a partition of unity is used to localize a globally-defined data is choosing suitable tolerances* $\{TOL_i\}$ *for the localized computations for* $\{\hat{U}_i\}$. *Using* $TOL_i \equiv TOL/N$ *as in (4.9), where* N *is the number of domains in the partition and* TOL *is the specified error tolerance for the data* ψ, *certainly guarantees that the partition of unity solution* U_p *obtained by combining the* $\{\hat{U}_i\}$ *has the required accuracy. But, this pessimistically assumes that there is no cancellation of the errors of the localized solutions* $\{\hat{U}_i\}$ *when they are combined to form* U_p. *In practice, this appears to be much too conservative.*

We adopt the strategy of choosing the local tolerances $\{TOL_i\}$ *so that the estimate of the accuracy of the final partition of unity solution* U_p *is close to the estimate of the accuracy of the solution of the Global Computation. We begin with the same tolerance used for the Global Computation and then decrease it if necessary. It seems likely that it would be more efficient to monitor the accuracy of the localized solutions and decrease the tolerance as necessary at each step of the solution-estimation-refinement process. However, while simple to implement, the resulting adaptive algorithm is complicated and demands further analysis.*

For the first Decomposed Computation, we obtain acceptable results using the same tolerance of 5% as used for the Global Computation. Details of the final computed solutions are listed below:

Data	Level	Elements	Estimate
ψ_1	3	618	.01242
ψ_2	3	575	−.0009109
ψ_3	3	618	.01242
ψ_4	3	575	−.0009109

Combining these solutions yields a partition of unity solution U_p with accuracy .023. Using the Decomposed Computation yields a Final Element Ratio of $3505/618 \approx 5.7$.

We plot the final meshes for two of the computations in Fig. 7.4. To visualize the effects of the

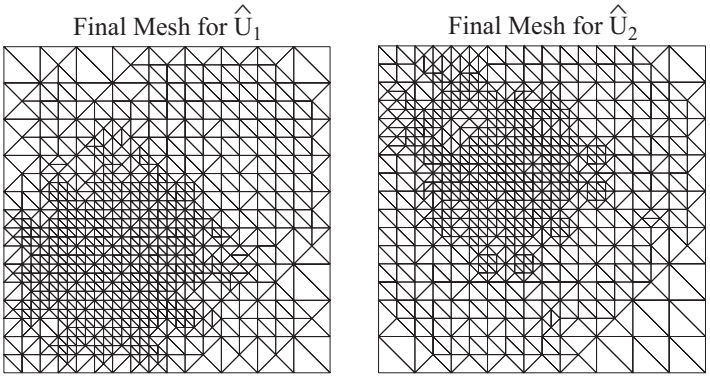

FIG. 7.4. *Final meshes for* $\hat{U}_1$ *and* $\hat{U}_2$ *for Example 1 with a partition of unity on four domains.*

decay of influence, we plot the generalized Green's functions for the global average error and the localized solution corresponding to ψ_2 in Fig. 7.5. The decay of influence away from the support of ψ_2 is clearly visible in the solution on the right.

Next, we perform a Decomposed Computation using a partition of unity approximation on the 16 equal-sized regions shown in Fig. 7.6. We again use an error tolerance of 5% and start the localized computations with the same initial 10×10 mesh used above. Computing the correlation ratios, we find these significant correlations:

$$\mathcal{E}_2 \text{ with } \mathcal{E}_3 \quad \mathcal{E}_5 \text{ with } \mathcal{E}_8 \quad \mathcal{E}_{10} \text{ with } \mathcal{E}_9 \quad \mathcal{E}_{13} \text{ with } \mathcal{E}_{14}$$
$$\mathcal{E}_4 \text{ with } \mathcal{E}_3 \quad \mathcal{E}_7 \text{ with } \mathcal{E}_8 \quad \mathcal{E}_{12} \text{ with } \mathcal{E}_9 \quad \mathcal{E}_{15} \text{ with } \mathcal{E}_{14}$$

This suggests that we should see less gain from the decay of influence when using this partition.

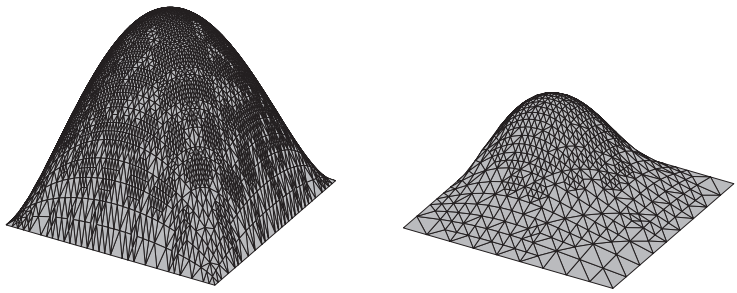

FIG. 7.5. *The generalized Green's functions for the global average error and the localized solution $\hat{U}_2$ corresponding to ψ_2 with a partition of unity on four domains.*

6	7	10	11
5	8	9	12
2	3	14	15
1	4	13	16

FIG. 7.6. *Domains for the second partition of unity used in Example 1.*

We report the results for the accepted approximations:

Data	Level	Elements	Estimate	Data	Level	Elements	Estimate
ψ_1	2	187	−.0005256	ψ_9	4	1371	−.006256
ψ_2	3	560	.002904	ψ_{10}	3	560	.002904
ψ_3	4	1371	−.006256	ψ_{11}	2	187	−.0005256
ψ_4	3	560	.002904	ψ_{12}	3	560	.002904
ψ_5	3	569	.001520	ψ_{13}	3	569	.001520
ψ_6	2	212	.002566	ψ_{14}	4	1285	−.009831
ψ_7	3	569	.001520	ψ_{15}	3	569	.001520
ψ_8	4	1285	−.009831	ψ_{16}	2	212	.002566

In order to obtain an acceptable accuracy in the four sub-domains closest to the center, we have to use an extra refinement level in the computation of the corresponding local solutions. The error in the average of the resulting partition of unity solution is .011. If we use the Decomposed Computation, the most intensive individual computations are those for ψ_3 and ψ_9, which yields a Final Element Ratio of $3505/1371 \approx 2.6$. There is still a significant gain over the Global Computation, but not as large as gain as using a partition with four sub-domains.

7.2. Example 2. In the second experiment, we estimate the error in some point values and the average value of u solving

$$\begin{cases} -\nabla \cdot \big((1.1 + \sin(\pi x)\sin(\pi y))\nabla u(x,y)\big) \\ \qquad = -3\cos^2(\pi x) + 4\cos^2(\pi x)\cos^2(\pi x) \\ \qquad\quad +2.2\sin(\pi x)\sin(\pi y) + 2 - 3\cos^2(\pi y), & (x,y) \in \Omega, \\ u(x,y) = 0, & (x,y) \in \partial\Omega, \end{cases} \tag{7.2}$$

where $\Omega = [0,2] \times [0,2]$ and the exact solution is $u(x,y) = \sin(\pi x)\sin(\pi y)$. We compute the average error corresponding to $\psi_1 \equiv 1/4$ and then four point values corresponding to $\psi_2 \approx \delta_{(.5,.5)}$, $\psi_3 \approx \delta_{(.5,1.5)}$, $\psi_4 \approx \delta_{(1.5,1.5)}$, and $\psi_5 \approx \delta_{(1.5,.5)}$. We use

$$\hat{\delta}_{(c_x,c_y)} = \frac{400}{\pi} e^{-400((x-c_x)^2+(y-c_y)^2)}$$

to approximate the delta function $\delta_{(c_x,c_y)}$.

In the Global Computation, we compute a mesh that gives all of the desired information accurately using a tolerance of 2%. We begin with an 8×8 mesh. We list the results below:

		ψ_1			ψ_2			ψ_3		
Lev.	Elt's	Est.	Err.	Rat.	Est.	Err.	Rat.	Est.	Err.	Rat.
1	64	.035	.035	1.0	.090	.29	3.3	.24	.022	.091
2	201	.0088	.0089	1.0	.042	.082	1.9	.0024	.014	6.0
3	763	.0027	.0027	1.0	.020	.020	.99	.0020	.0020	1.0
4	2917	.00044	.00044	1.0	.0050	.00504	1.0	.0049	.00504	1.0

The error estimates for the point values are not very accurate on the coarser meshes, but become very accurate on mesh of moderate density and finer. It is simply an issue of locating a sufficient number of elements near the centers of the delta functions so that the approximation of the generalized Green's functions is accurate.

We obtain an acceptably accurate solution after four refinement levels using a mesh with 2917 elements. We plot both the initial and final meshes in Fig. 7.7.

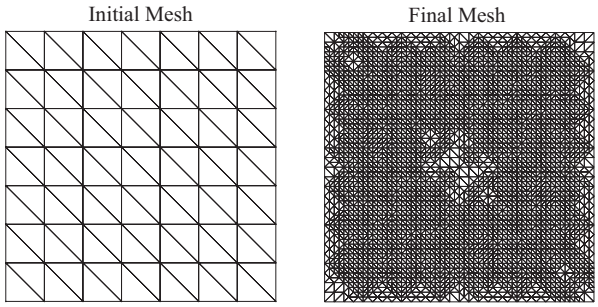

FIG. 7.7. *Initial and final meshes for Example 2 with for the solution computing all five data.*

We next perform a Decomposed Computation by solving for approximate solutions $\{\hat{U}_1, \cdots, \hat{U}_5\}$ corresponding to each data $\{\psi_1, \cdots, \psi_5\}$ independently. Checking the Correlation Ratios reveals no significant correlations between the independent error indicators. There is no partition of unity involved in this decomposition and we simply use the same tolerance 2% for each independent computation. However, to obtain final independent solutions that yield roughly the same accuracy in the computed quantities as the solution of the Global Computation, we vary the initial meshes; using 7×7 for $\hat{U}_1$; 9×9 for $\hat{U}_2$ and $\hat{U}_4$; and 12×12 for $\hat{U}_3$ and $\hat{U}_5$. The final results for each computation are listed below:

Data	Level	Elements	Estimate
ψ_1	3	409	$-.0004699$
ψ_2	4	1037	$-.007870$
ψ_3	2	281	$-.005571$
ψ_4	4	1037	$-.007870$
ψ_5	2	281	$-.005571$

The Final Element Ratio is $2917/1037 \approx 2.8$. Since the solution corresponding to the average error is not the dominant cost in the independent computations, we do not bother to do a partition of unity decomposition on that problem. Finally, we plot some of the final meshes in Fig. 7.8.

7.3. Example 3. In this section, we investigate some properties of the correlation indicators using the problem,

$$\begin{cases} -\Delta u = 16(y - y^2 + x - x^2) & (x,y) \in \Omega, \\ u(x,y) = 0, & (x,y) \in \partial\Omega, \end{cases} \tag{7.3}$$

where $\Omega = [0,1] \times [0,1]$ and the exact solution is $u(x,y) = 8x(1-x)y(1-y)$.

In the two examples considered so far, there has been little or no significant correlation in the error indicators of different data, and computing the corresponding solutions independently leads to a substantial gain in terms of decreasing the maximum number of elements required to achieve a desired accuracy in specified quantities of interest. In the first computation in this example, we consider a problem in which two data are substantially correlated.

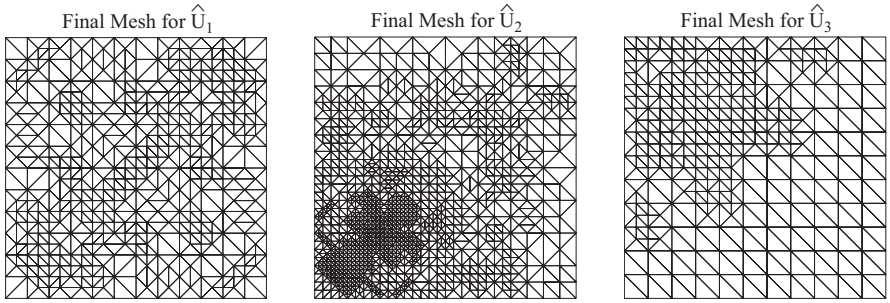

FIG. 7.8. *Final meshes for* $\{\hat{U}_1, \hat{U}_2, \hat{U}_3\}$ *in Example 2. The mesh for* $\hat{U}_4$ *is symmetric across* $y = 2 - x$ *with the mesh for* $\hat{U}_2$ *and the mesh for* $\hat{U}_5$ *is symmetric across* $y = x$ *with the mesh for* $\hat{U}_3$.

We estimate the error in the average value of u solving (7.3). Since the domain is relatively small and the solution and the generalized Green's function are both very smooth, the gain from decomposing the solution using a partition of unity is greatly reduced compared the previous examples. Beginning with a 4×4 mesh and using a tolerance of 1%, we obtain a sufficiently accurate solution using a Global Computation after five refinements. The final mesh uses 885 elements and produces an error of .0008699. If we partition the domain using four equal regions as pictured in Fig. 7.3, we find no substantial correlations between the error indicators $\{\mathcal{E}_1, \cdots, \mathcal{E}_4\}$. Computing the four solutions independently in the Decomposed Computation yields a Final Element Ratio of around 1.5.

If we partition the domain using sixteen equal regions as pictured in Fig. 7.6, we find a number of substantial correlations. For example, we find that

Correlation Ratio 1 for $\mathcal{E}_1$ on $\mathcal{E}_2 = .98$, Correlation Ratio 2 for $\mathcal{E}_1$ on $\mathcal{E}_2 = .44$,
Correlation Ratio 1 for $\mathcal{E}_2$ on $\mathcal{E}_1 = .82$, Correlation Ratio 2 for $\mathcal{E}_2$ on $\mathcal{E}_1 = .44$.

Computing $\hat{U}_1$ corresponding to the localized data ψ_1 using a tolerance of 1% we obtain a sufficiently accurate solution after 5 refinements, producing a mesh with 367 elements and yielding an error estimate of $-.000047$. Repeating the computation for $\hat{U}_2$ also requires five refinements, producing a mesh with 494 elements and yielding an accuracy of $-.000066$. On the other hand, combining these two computations by using data equal to the sum of the two partition functions for the regions Ω_1 and Ω_2, results in a problem that requires 5 refinements, producing a mesh with 496 elements and an accuracy of $-.000097$. Thus, we gain almost nothing by computing $\hat{U}_1$ and $\hat{U}_2$ independently from each other. We plot the final meshes in Fig. 7.9.

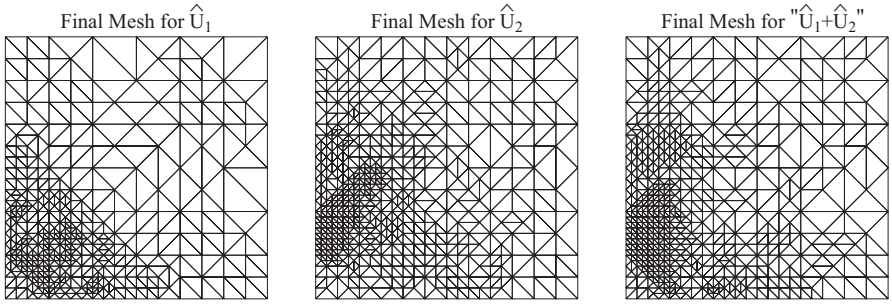

FIG. 7.9. *Final meshes for* $\hat{U}_1$, $\hat{U}_2$, *and the "combined" solution in Example 3.*

In the second computation in this example, we investigate the effect on the robustness of the Correlation Indicators from computing the Indicators on coarse discretizations. We consider the error in the average value and the point values at $(.25, .25)$ and $(.5, .5)$. We use a partition of unity decomposition for the error in the average to get data $\{\psi_1, \cdots, \psi_4\}$. We let $\psi_5 \approx \delta_{(.25,.25)}$ and $\psi_6 \approx \delta_{(.5,.5)}$. We compare the correlation indicators on initial meshes ranging from 16 to 144 or 400 uniformly sized elements by plotting the Correlation Ratios versus the number of elements.

We show a sample of results in Fig. 7.10.

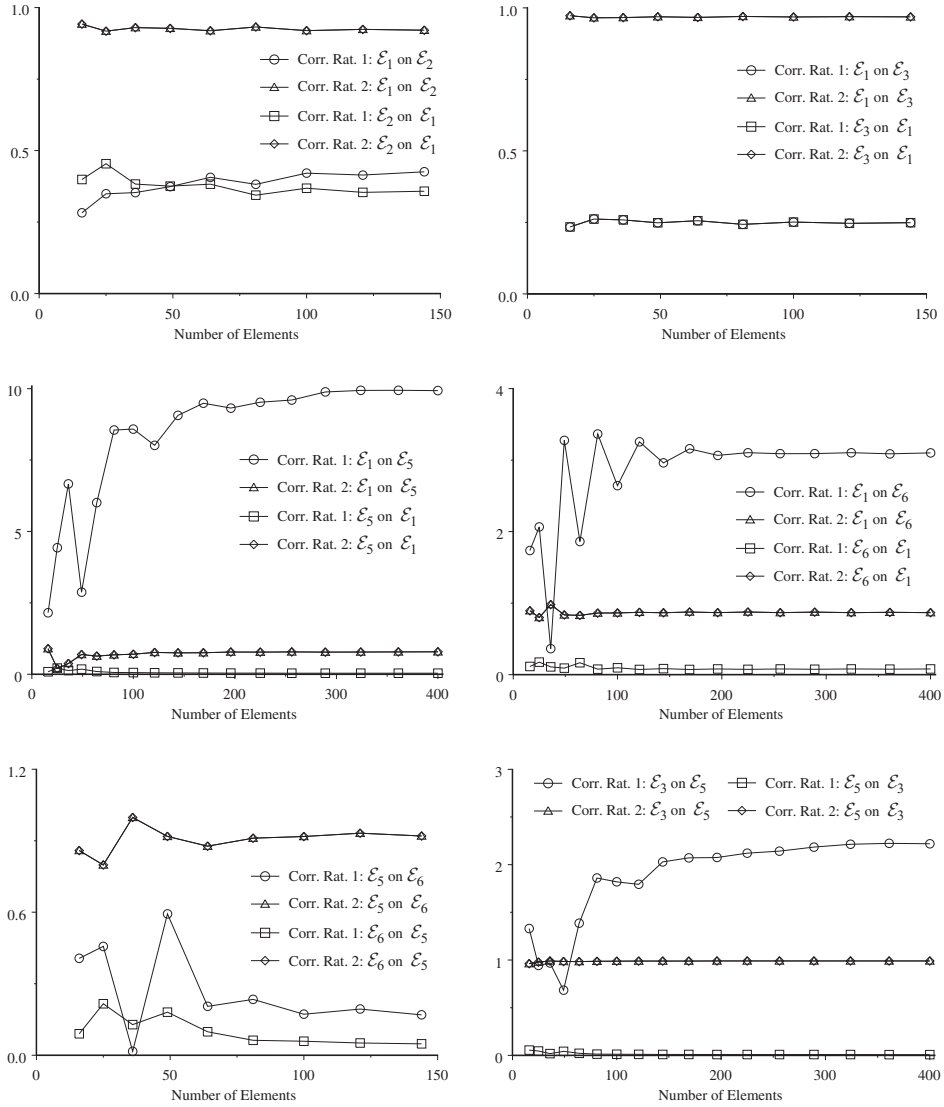

FIG. 7.10. *Plots of Correlation Ratios for a sample of computations in Example 3.*

In general, we find that all Correlation Ratios converge to a limit as the number of elements increases (and we can actually prove this is so). What is more important however is the degree of variation on coarse meshes. Generally, the second Correlation Ratio varies relatively little as the mesh density increases for all data. The first Correlation Ratio between data representing a partition of unity decomposition also varies relatively little. However, it is not surprising to see that the first Correlation Ratio varies quite a bit on coarse meshes when one of the data is an approximate delta function. In terms of determining significant correlation, we find that the determination that two effective domains of influence are *not* closely correlated seems to be relatively robust with respect to the density of the mesh on which the indicators are computed. The determination that two effective domains of influence are correlated is less robust. Practically, this means that there is a mild tendency to combine computations that are more efficiently treated independently if the correlation indicators are computed on very coarse meshes.

7.4. Example 4. We turn to consider some problems for which we can not expect to obtain precise analytic information about the generalized Green's function. In this example, we consider

a problem with diffusion that is nearly singular at one point and that has strong convection. We estimate the error in the average value of u solving

$$\begin{cases} -\nabla \cdot \big(\big(.05 + \tanh\big(10(x-5)^2 + 10(y-1)^2\big)\big) \nabla u \big) \\ \qquad\qquad + \begin{pmatrix} -100 \\ 0 \end{pmatrix} \cdot \nabla u = 1, & (x,y) \in \Omega, \\ u(x,y) = 0, & (x,y) \in \partial\Omega, \end{cases} \tag{7.4}$$

where $\Omega = [0,10] \times [0,2]$. We plot the diffusion in Fig. 7.11. Because of the sign of the convec-

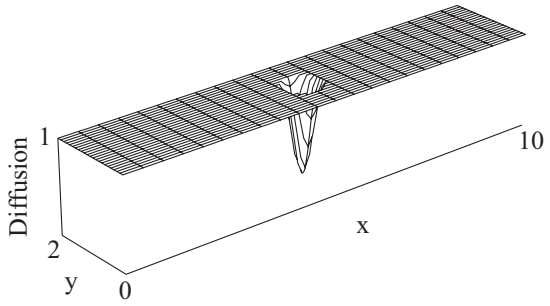

FIG. 7.11. *Plot of the diffusion coefficient for Example 4.*

tion, we expect that perturbations to the solution at a point with x-coordinate x_0 will affect the solution's values "downstream" for $x < x_0$ most strongly. The Peclet number for this problem is $Pe = 1000$.

We begin the computations with an initial mesh of 80 elements. For the Global Computation, we use an error tolerance of $TOL = .04\%$. We list some details of the computation below:

Level	Elements	Estimate
1	80	−.0005919
2	193	−.001595
3	394	−.0009039
4	828	−.0003820
5	1809	−.0001070
6	3849	−.00004073
7	9380	−.00001715
8	23989	−.000007553

We plot the final mesh in Fig. 7.12. The effects of the convection are clear in the pattern of mesh

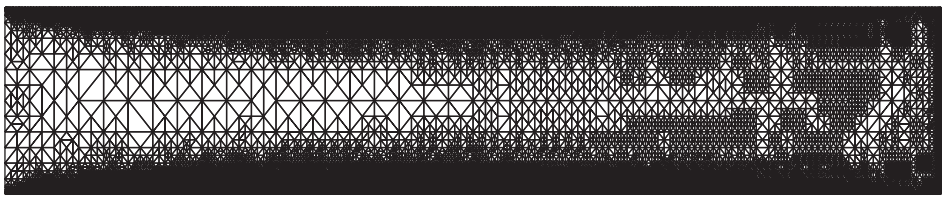

FIG. 7.12. *Plot of the final mesh for Example 4 with data ψ giving the average error.*

refinement. For the sake of comparison, we compute a numerical solution of the same problem except posing a velocity vector of $b = (-.01, 0)^\top$, corresponding to a Peclet number $Pe = .1$. We plot meshes from the original computation and the altered problem of approximately the same number of elements in Fig. 7.13. In the altered problem, the mesh refinement is much more heterogeneous.

Next, we consider the partition of unity with 20 subdomains shown in Fig. 7.14. Computing the Correlation Ratios, we find the significant correlations:

$\mathcal{E}_3$ with $\mathcal{E}_4$ $\quad$ $\mathcal{E}_6$ with $\mathcal{E}_7$ $\quad$ $\mathcal{E}_7$ with $\mathcal{E}_6$ $\quad$ $\mathcal{E}_9$ with $\mathcal{E}_8$ $\quad$ $\mathcal{E}_{10}$ with $\mathcal{E}_8$, $\mathcal{E}_9$

$\mathcal{E}_{13}$ with $\mathcal{E}_{14}$ $\quad$ $\mathcal{E}_{16}$ with $\mathcal{E}_{17}$ $\quad$ $\mathcal{E}_{17}$ with $\mathcal{E}_{16}$ $\quad$ $\mathcal{E}_{19}$ with $\mathcal{E}_{18}$ $\quad$ $\mathcal{E}_{20}$ with $\mathcal{E}_{18}$, $\mathcal{E}_{19}$

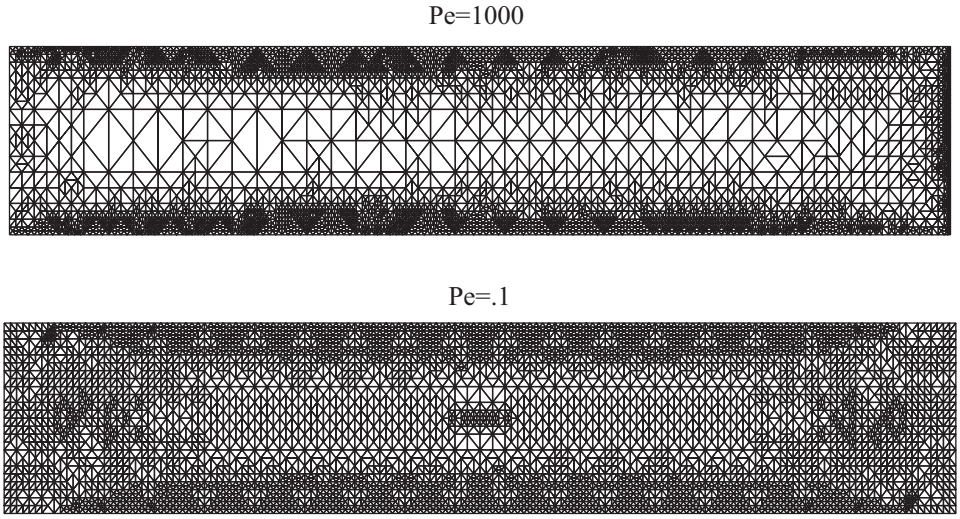

FIG. 7.13. *Plots of the mesh in the original problem with* $Pe = 1000$ *at refinement level* 6 *(number of elements* $= 3849$ *and the altered problem with* $Pe = .1$ *(number of elements* $= 4192$*) for Example 4 with data* ψ *giving the average error. We display the meshes from early refinement levels to make the qualitative features of the refinement clearer.*

11	12	13	14	15	16	17	18	19	20
1	2	3	4	5	6	7	8	9	10

FIG. 7.14. *Domains for the partition of unity used in Example 4.*

Note, there are no significant correlations in the cross-wind direction.

We compute the localized solutions $\{\hat{U}_i\}$ in the Decomposed Computation using two tolerances. The solutions are completely symmetric across $y = 1$. Details of the final computed solutions are listed below:

Data	TOL	Level	Elements	Estimate
ψ_1	.04%	7	7334	-6.927×10^{-7}
ψ_2	.04%	7	8409	-5.986×10^{-7}
ψ_3	.04%	7	7839	-5.189×10^{-7}
ψ_4	.04%	7	7177	-5.306×10^{-7}
ψ_5	.04%	7	7301	-4.008×10^{-7}
ψ_6	.02%	7	6613	-2.471×10^{-7}
ψ_7	.02%	7	4396	-2.938×10^{-7}
ψ_8	.02%	7	4248	-1.656×10^{-7}
ψ_9	.02%	7	3506	-1.221×10^{-7}
ψ_{10}	.02%	7	1963	-5.550×10^{-8}

The estimate on the total average error of U_p is 7.24×10^{-6} and the Final Element Ratio is $23909/8409 \approx 2.9$.

We show a sample of the final meshes for the Decomposed Computation in Fig. 7.15. Note the effect of the convection is clearly visible in the pattern of mesh refinement. We can also see this in the graphs of the generalized Green's functions. We plot a sample in Fig. 7.16. Note the support of the two functions.

REMARK 7.5. *In Sec. 4, we emphasized that effective domains of influence may not be spatially compactly-shaped, as generally occurs for Poisson's equation. We can see this clearly in the upper plot in Fig. 7.15. The effective domain of influence for the average value of the solution in the lower left corner of the domain, close to the outflow boundary at* $x = 0$*, contains the immediate neighborhood of the boundary along* $y = 0$*, a swath that cuts up from the center of the outflow boundary through the center of the domain up to the upper boundary, and most of the inflow*

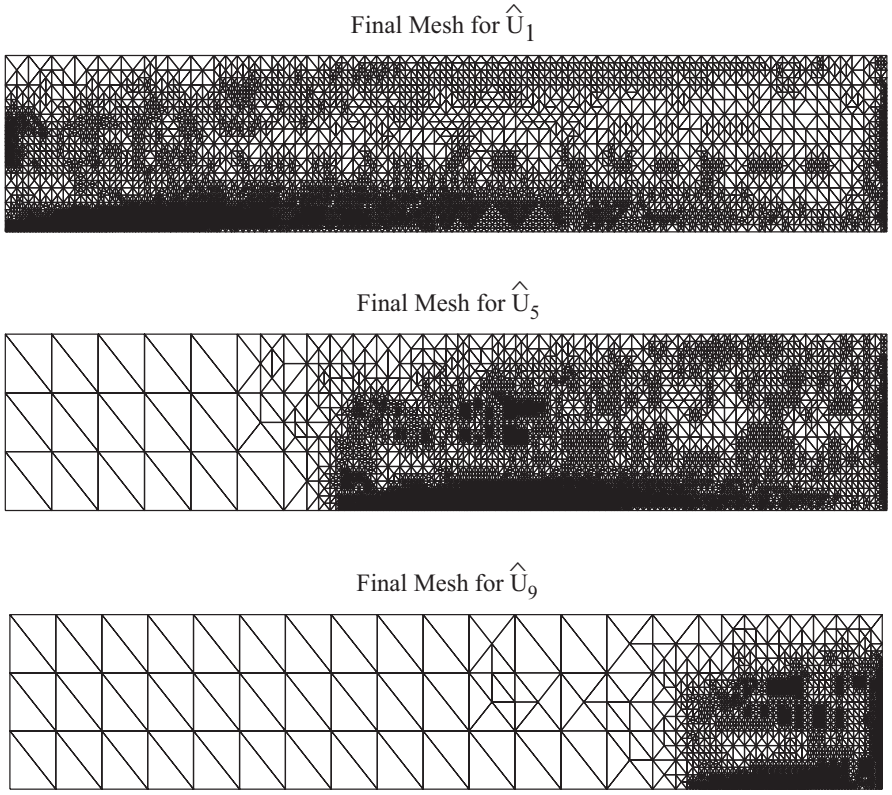

FIG. 7.15. *Plots of the final meshes for the localized solutions $\hat{U}_1$, $\hat{U}_5$, and $\hat{U}_9$ in Example 4.*

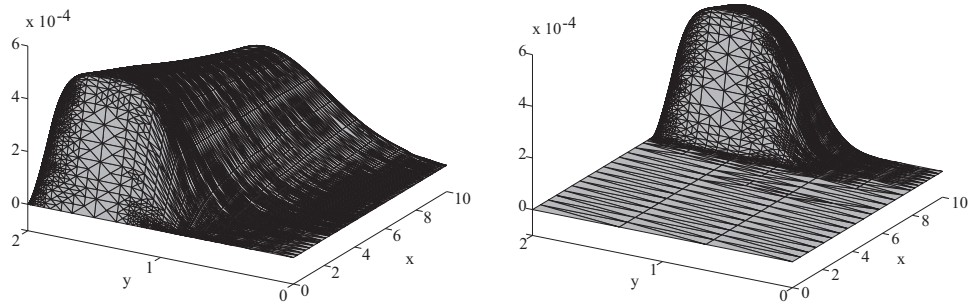

FIG. 7.16. *Plots of the generalized Green's functions corresponding to ψ_{11} (left) and ψ_{19} (right) in Example 4.*

boundary.

Keeping in mind the significant correlations listed above, we combine some of the localized computations by solving for localized solutions corresponding to summing the two of the partition of unity data. We list details of the final computed solutions below:

Data	TOL	Level	Elements	Estimate
$\psi_3 + \psi_4$	.04%	7	8330	-9.8884×10^{-7}
$\psi_6 + \psi_7$	.02%	7	5951	-5.897×10^{-7}
$\psi_8 + \psi_9$	.02%	7	4406	-3.486×10^{-7}
$\psi_9 + \psi_{10}$	.02%	7	3202	-2.243×10^{-7}

The solutions for $\psi_3 + \psi_4$ and $\psi_8 + \psi_9$ use a few more elements than required for either of the original localized solutions. The solutions for $\psi_6 + \psi_7$ and $\psi_9 + \psi_{10}$ use less than the maximum required for the individual localized solutions.

7.5. Example 5. In the last example, we consider a problem posed on a more complicated domain. We estimate the error in the average value of u solving

$$\begin{cases} -\frac{1}{\pi^2}\Delta u = 2 + 4e^{-5((x-.5)^2+(y-2.5)^2)}, & (x,y) \in \Omega, \\ u(x,y) = 0, & (x,y) \in \partial\Omega, \end{cases} \tag{7.5}$$

where Ω is the "square annulus" $\Omega = [0,3] \times [0,3] \setminus [1,2] \times [1,2]$. The domain Ω is shown in Fig. 7.19. Note that we introduce some local variation in the forcing to make the solution more interesting.

We begin the computations with an initial mesh of 48 elements. For the Global Computation, we use an error tolerance of $TOL = 1\%$. We list some details of the computation below:

Level	Elements	Estimate
1	48	−5.168
2	125	−1.584
3	380	−.6879
4	894	−.3029
5	2075	−.1435

We plot the initial and final meshes in Fig. 7.17. Note the expected refinement required near the

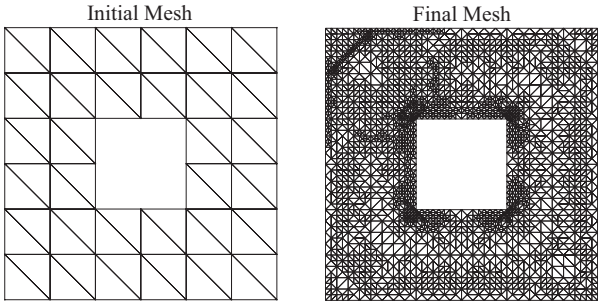

FIG. 7.17. *Plots of the initial (left) and final (right) meshes for Example 5 with data ψ giving the average error.*

interior corners. We plot the final solution and generalized Green's function in Fig. 7.18.

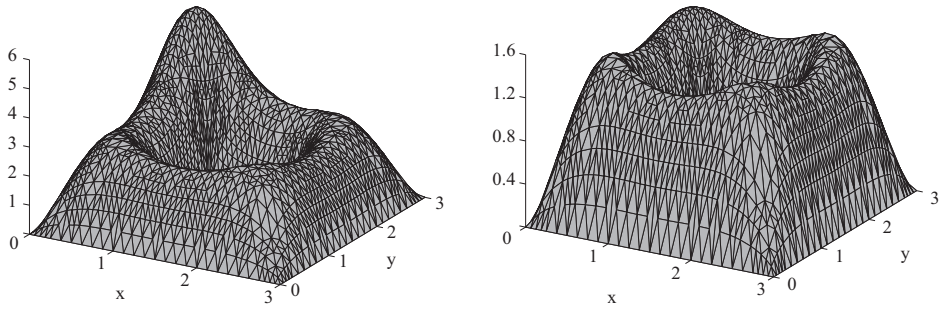

FIG. 7.18. *Plots of the final solution (left) and generalized Green's function (right) for Example 5 with data ψ giving the average error.*

Next, we consider the partition of unity with 8 subdomains shown in Fig. 7.19. Checking the Correlation Ratios reveals no significant correlations. We obtain acceptable results in the Decomposed Computation using the same tolerance of 1% as used for the Global Computation. Details of the final computed solutions are listed below:

Data	Level	Elements	Estimate	Data	Level	Elements	Estimate
ψ_1	5	1082	−.01935	ψ_5	5	1104	−.01436
ψ_2	5	1101	−.01399	ψ_6	5	1110	−.01587
ψ_3	5	1144	−.01540	ψ_7	5	1074	−.02529
ψ_4	5	1107	−.01360	ψ_8	5	1098	−.01660

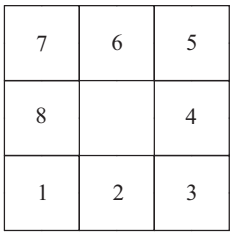

FIG. 7.19. *Domains for the partition of unity used in Example 5.*

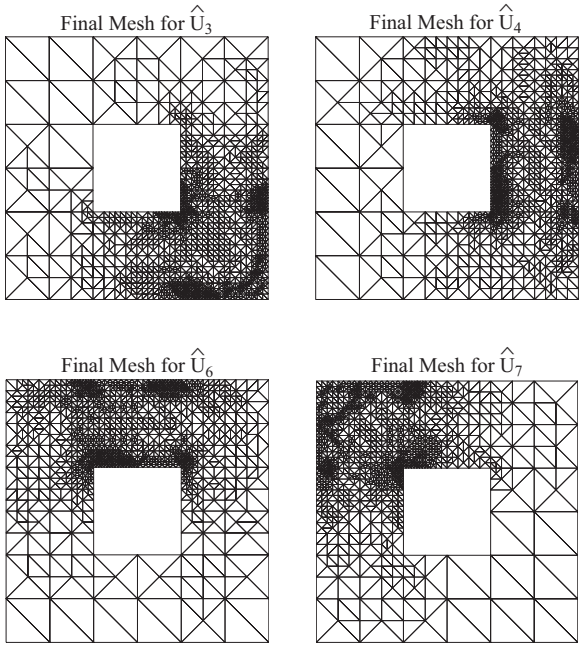

FIG. 7.20. *Plots of the final meshes for the localized solutions $\hat{U}_3$, $\hat{U}_4$, $\hat{U}_6$, and $\hat{U}_7$ in Example 5.*

Combining these solutions yields a partition of unity solution U_p with accuracy $-.1344$. Using the Decomposed Computation yields a Final Element Ratio of ≈ 1.8. We show a sample of the final meshes in Fig. 7.20. The most significant factor leading to a reduction in the number of elements required to achieve a desired accuracy is the fact that the localized computations do not refine near corners that are not in the immediate neighborhood of the support of the data.

We plot a couple of the final generalized Green's functions in Fig. 7.21.

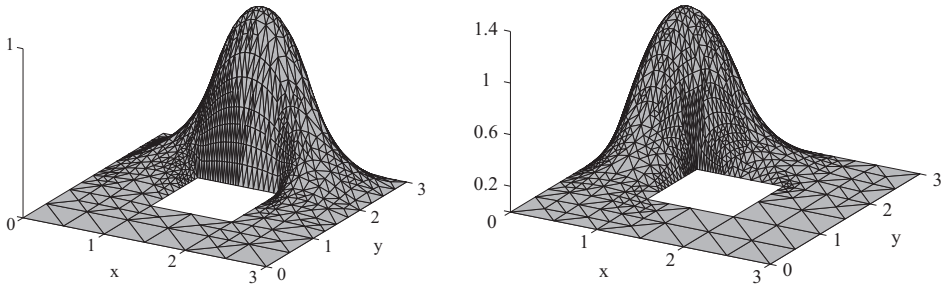

FIG. 7.21. *Plots of the generalized Green's functions corresponding to ψ_6 (left) and ψ_7 (right) for the partition of unity decomposition for Example 5.*

We also tried a partition of unity on a finer decomposition of Ω obtained by dividing each

sub-domain in the first partition into four equal squares. However, the Final Element Ratio is only 1.09.

8. Conclusion. There are a number of approaches to selecting elements for refinement in adaptive mesh refinement, though the goal is always the same: compute an accurate solution at a relatively low cost, e.g., in terms of execution time or memory. In most approaches, there is no pretense at controlling an actual error, either because there is no underlying global error estimate or because any underlying error estimate is so inaccurate as to be effectively useless. Rather the elements are chosen for refinement in order to decrease some measure of the discretization error, such as truncation error or residual. This generally works well. After all, ultimately the only guaranteed way to improve the accuracy of a computed solution is to decrease the discretization error, for example, by refining the mesh.

In contrast, the advantage of the approach to adaptive mesh refinement described in this paper is that it depends on an *a posteriori* analysis that actually attempts to estimate the true error in a quantity of interest. It does this by taking into account the behavior of the generalized Green's function associated to the quantity of interest. The generalized Green's function determines the global effects of local discretization error on the true solution. The cost can be considerable, as this approach involves numerically solving the adjoint problem in most cases. The payoff is accuracy of the estimate and therefore reliability in the results.

What we shown in this paper is that the additional information obtained by approximating the generalized Green's function can be used to actually improve the efficiency of the solution process. This possibility arises when the goal is to compute multiple quantities of interest and/or to compute quantities of interest that involve globally-supported information of the solution, as with average values and norms. In the latter case, we introduce a decomposition of solution that localizes the global computation by replacing it by a set of problems involving localized information. The decomposition allows recovery of the desired information by combining the local solutions. By treating each computation of a quantity of interest as an independent computation, we can reduce the maximum number of elements required to achieve a specified accuracy in the specified quantities of interest. This in turn can lead to a significant decrease in solution time in the setting of coarse-grained parallelization and a memory-constrained computing environment.

In general, it is difficult to quantify the potential gain in efficiency due to the proposed approach. However, we have demonstrated that significant reductions in the maximum number of elements required to achieve a specified accuracy are possible in a variety of situations using one analytic example and a series of computations. Moreover, the nature of elliptic problems means that we can expect even larger reduction if we consider problems posed on three dimensional spatial domains and/or on problems posed on domains that are complicated and large.

REFERENCES

[1] I. Babuška and J. Melenk, *The partition of unity finite element method*, Internat. J. Numer. Methods Engrg., 40 (1997), pp. 727–758.

[2] R. Bank and M. Holst, *A new paradigm for parallel adaptive mesh refinement*, SIAM J. Sci. Comput., 22 (2000), pp. 1411–1443.

[3] R. Becker and R. Rannacher, *An optimal control approach to a posteriori error estimation in finite element methods*, Acta Numerica, (2001), pp. 1–102.

[4] S. Brenner and L. R. Scott, *The Mathematical Theory of Finite Element Methods*, Springer-Verlag, New York, 1994.

[5] L. Dieci and D. Estep, *Some stability aspects of schemes for the adaptive integration of stiff initial value problems*, SIAM J. Sci. Stat. Comput., 12 (1991), pp. 1284–1303.

[6] K. Eriksson, D. Estep, P. Hansbo, and C. Johnson, *Introduction to adaptive methods for differential equations*, Acta Numerica, (1995), pp. 105–158.

[7] ———, *Computational Differential Equations*, Cambridge University Press, New York, 1996.

[8] K. Eriksson and C. Johnson, *Adaptive finite element methods for parabolic problems I: A linear model problem*, SIAM J. Numer. Anal., 28 (1991), pp. 43–77.

[9] D. Estep, *A posteriori error bounds and global error control for approximations of ordinary differential equations*, SIAM J. Numer. Anal., 32 (1995), pp. 1–48.

[10] D. Estep and M. Holst, *FETkLab: Finite Element Toolkit for MATLAB*, 2002. can be obtained from http://www.fetk.org.

[11] D. Estep, M. Holst, and D. Mikulencak, *Accounting for stability:* a posteriori *error estimates based on residuals and variational analysis*, Comm. Num. Meth. Engin., 18 (2002), pp. 15–30.
[12] D. J. Estep and M. G. Larson, *A theoretical framework for computational error estimation in linear elliptic problems via a variational a posteriori error analysis.* in preparation, 2002.
[13] D. J. Estep, M. G. Larson, and R. D. Williams, *Estimating the error of numerical solutions of systems of reaction-diffusion equations*, Memoirs A.M.S., 146 (2000), pp. 1–109.
[14] G. Folland, *Introduction to Partial Differential Equations*, Princeton University Press, Princeton, New Jersey, 1995.
[15] M. Giles and E. Süli, *Adjoint methods for pdes: a posteriori error analysis and postprocessing by duality*, Acta Numerica, (2002), pp. 145–236.
[16] M. Griebel and M. Schweitzer, *A particle-partition of unity method for the solution of elliptic, parabolic, hyperbolic pdes*, SIAM J. Sci. Comput., 22 (2000), pp. 853–890.
[17] M. Holst, *Adaptive numerical treatment of elliptic systems on manifolds*, Adv. Comput. Math., 15 (2001), pp. 139–191.
[18] ———, *Applications of domain decomposition and partition of unity methods in physics and geometry (plenary paper)*, in Fourteenth International Conference on Domain Decomposition Methods, January 2002, Mexico City, Mexico, 2002.
[19] C. Johnson, S. Larsson, V. Thomée, and L. Wahlbin, *Error estimates for spatially discrete approximations of semilinear parabolic equations with nonsmooth initial data*, Math. Comput., 49 (1987), pp. 331–357.
[20] J. Lions and E. Magenes, *Non-Homogeneous Boundary Value Problems and Applications*, vol. 1, Springer-Verlag, New York, 1972.
[21] J. Xu and A. Zhou, *Local and parallel finite element algorithms based on two-grid discretizations*, Math. Comput., 69 (2000), pp. 881–909.

Chalmers Finite Element Center Preprints

2001–01 *A simple nonconforming bilinear element for the elasticity problem*
Peter Hansbo and Mats G. Larson

2001–02 *The $\mathcal{LL}^*$ finite element method and multigrid for the magnetostatic problem*
Rickard Bergström, Mats G. Larson, and Klas Samuelsson

2001–03 *The Fokker-Planck operator as an asymptotic limit in anisotropic media*
Mohammad Asadzadeh

2001–04 *A posteriori error estimation of functionals in elliptic problems: experiments*
Mats G. Larson and A. Jonas Niklasson

2001–05 *A note on energy conservation for Hamiltonian systems using continuous time finite elements*
Peter Hansbo

2001–06 *Stationary level set method for modelling sharp interfaces in groundwater flow*
Nahidh Sharif and Nils-Erik Wiberg

2001–07 *Integration methods for the calculation of the magnetostatic field due to coils*
Marzia Fontana

2001–08 *Adaptive finite element computation of 3D magnetostatic problems in potential formulation*
Marzia Fontana

2001–09 *Multi-adaptive galerkin methods for ODEs I: theory & algorithms*
Anders Logg

2001–10 *Multi-adaptive galerkin methods for ODEs II: applications*
Anders Logg

2001–11 *Energy norm a posteriori error estimation for discontinuous Galerkin methods*
Roland Becker, Peter Hansbo, and Mats G. Larson

2001–12 *Analysis of a family of discontinuous Galerkin methods for elliptic problems: the one dimensional case*
Mats G. Larson and A. Jonas Niklasson

2001–13 *Analysis of a nonsymmetric discontinuous Galerkin method for elliptic problems: stability and energy error estimates*
Mats G. Larson and A. Jonas Niklasson

2001–14 *A hybrid method for the wave equation*
Larisa Beilina, Klas Samuelsson and Krister Åhlander

2001–15 *A finite element method for domain decomposition with non-matching grids*
Roland Becker, Peter Hansbo and Rolf Stenberg

2001–16 *Application of stable FEM-FDTD hybrid to scattering problems*
Thomas Rylander and Anders Bondeson

2001–17 *Eddy current computations using adaptive grids and edge elements*